Form of opening (renewal) for Project

APPROVED
JINR DIRECTOR

_____/

"____" _____ **202**__

PROJECT PROPOSAL FORM

Opening/renewal of a research project/subproject of the large research infrastructure project within the Topical plan of JINR

1. General information on the research project

1.1 Theme code - 02-1-1086-2009 Strangeness in Hadronic Matter and Study of Inelastic Reactions Near Kinematical Borders

1.2 Project (for extended projects)

1.3 Laboratory VBLHEP

1.4 Scientific field Particle physics and relativistic nuclear physics

1.5 Title of the project HyperNIS–SRC

1.6 Project leader(s) D. O. Krivenkov, J. Lukstins

1.7 Project deputy leader(s) (scientific supervisor(s)) M. A. Patsyuk

2. Scientific case and project organization

2.1 Annotation The experimental program of the joined HyperNIS–SRC project consists of two sections: HyperNIS and SRC.

The HyperNIS program is aimed at investigation of the role which strangeness plays in nuclei, namely open strangeness in hypernuclei. The HyperNIS program can be realized with the HyperNIS spectrometer. Taking into account the spectrometer capacity our efforts are concentrated on hypernuclear research. The goal of the program is the study of the lightest neutron-rich hypernuclei. In particular, it is necessary to establish firmly if the hypernucleus ${}^{6}_{\Lambda}\mathrm{H}$ really exists. It should be noted that in the same experiment the lifetimes and production cross sections of ${}^{4}_{\Lambda}\mathrm{H}$ and ${}^{3}_{\Lambda}\mathrm{H}$ will be investigated. The further experiment will be the study of ${}^{6}_{\Lambda}\mathrm{He}$, previously observed only in emulsion experiments. The next step of this program is aimed to determine the binding energy of the loosely bound ${}^{3}_{\Lambda}\mathrm{H}$ hypernucleus.

The SRC section present a two-phase research program aimed at investigating Short-Range Correlations (SRC) at the Joint Institute for Nuclear Research (JINR). In Phase 1, which spans the next 2-3 years, our focus will be on conducting measurements in the HyperNIS area. These measurements will involve the use of a polarized deuteron beam from the Booster/Nuclotron and existing detection

equipment at JINR. Specifically, we will explore polarized deuteron hard scattering off a liquid hydrogen target, with a focus on SRC kinematics. With a polarized deuteron beam of 6 GeV/c/nucleon momentum we will select interactions with $|t, u| > 1$ $(\mathrm{GeV/c})^2$, and a center-of-mass scattering angle around 90 degrees. A coincidence between the two arms of a dedicated spectrometer will identify two protons resulting from the p(d,2p)n reaction. Simultaneous detection of the recoil partner neutron arising from the deuteron's hard breakup will also be possible. The two-arm spectrometer will be akin to the one used in the 2022 SRC/BM@N measurement. Detection of the recoil neutron will necessitate the incorporation of a neutron detector along the beam. It is important to note that the installation of the required detection systems for Phase I measurements in the HyperNIS experimental area will not disrupt the existing HyperNIS experimental setup. Phase 2 of our research, also proposed to be conducted in the HyperNIS area, will focus on exclusive quasi-elastic scattering reactions in inverse kinematics with detection of the recoil fragment/fragments in coincidence. This phase requires extensive preparatory work, encompassing design and engineering efforts within the experimental area, and an investment in equipment. Both phases are an integral component of the global endeavor led by the international SRC collaboration to study dense nuclear systems and nucleon-nucleon interactions at close proximity, employing various reaction probes such as electrons, real photons, protons, and nuclei.

2.2 Scientific case (aim, relevance and scientific novelty, methods and approaches, techniques, expected results, risks)

HyperNIS

Aims of the project

The project is aimed to study the lightest neutron-rich hypernuclei; in particular, to search for and to study properties of ${}^{6}_{\Lambda}\mathrm{H}$. Simultaneously, lifetimes and production cross sections of ${}^{4}_{\Lambda}\mathrm{H}$ and ${}^{3}_{\Lambda}\mathrm{H}$ will be studied in the same experiment because we will use reaction

$$^{7}\mathrm{Li} + \mathrm{C} \rightarrow {}^{\mathrm{A}}_{\Lambda}\mathrm{H} + \mathrm{K} + \mathrm{p(d,t,n)} + \ldots \rightarrow {}^{\mathrm{A}}\mathrm{He} + \pi^{-} + \ldots, \quad (1)$$

where A = 3, 4, 6. Moreover, production and observation of ${}^{4}_{\Lambda}\mathrm{H}$ and ${}^{3}_{\Lambda}\mathrm{H}$ hypernuclei are the precise reference signal to make sure that ${}^{6}_{\Lambda}\mathrm{H}$ should be seen in the same run if it exists or that there are no stable forms of ${}^{6}_{\Lambda}\mathrm{H}$ if the last will not be observed. This task is regarded as the very first experiment because at Frascati experiment [1, 2, 3] evidence of only three events was reported and controversial data were obtained at J-PARC [4], where no signal was detected instead of expected 50 events.

The result of the ${}^{6}_{\Lambda}\mathrm{H}$ hypernucleus search should be a turning point of our program. If the ${}^{6}_{\Lambda}\mathrm{H}$ production cross section is high enough and the event yield is large, one should choose between two ways: either to continue the study of ${}^{6}_{\Lambda}\mathrm{H}$ properties or to search for the ${}^{8}_{\Lambda}\mathrm{H}$ hypernucleus. It seems that the search of and the possible discovery of the ${}^{8}_{\Lambda}\mathrm{H}$ hypernucleus will be the best decision. Particularly, since it is a very difficult task to investigate ${}^{8}_{\Lambda}\mathrm{H}$ using pion or kaon beams. The results of these two experiments will determine if it is better to study properties of the new hypernuclei or to turn to the ${}^{6}_{\Lambda}\mathrm{He}$ and ${}^{3}_{\Lambda}\mathrm{H}$ hypernucleus program.

The second way is also very rewarding. The study of the poorly investigated hypernucleus ${}^{6}_{\Lambda}\mathrm{He}$ will be a natural continuation of lithium beam experiments. With carbon beams, the program can be extended to determine the effective Hamiltonian of the $\Lambda\mathrm{N}\rightarrow\mathrm{NN}$ weak interaction.

One more original and attractive idea is the experimental estimation of the binding energy of the loosely bound ${}^{3}_{\Lambda}\mathrm{H}$ hypernucleus. Here the approach suggested in the Laboratory of High Energies (JINR, Dubna) will be used. In this approach the hypernuclei under study are being produced by an excitation of the beam nuclei and the hypernuclei decay is being observed at a distance of tens

of centimeters behind the production target. Thus, the passage of the hypernuclei "beam" through materials with different nuclear charges, Z, can be investigated to estimate the ${}^{3}_{\Lambda}$H binding energy. The primary ^{4}He beam is the best source for the ${}^{3}_{\Lambda}$H.

Introduction and physics motivation

The Hypernuclear program at Dubna [5, 6] was started in 1988 with the setup based on 2-m streamer chamber. The investigation of the light hypernuclei production and decay [6] was done, namely, the lifetime of ${}^{4}_{\Lambda}$H and ${}^{3}_{\Lambda}$H as well as their production cross sections were measured. It was shown that the approach in which the momentum of hypernuclei produced in the beams of relativistic ions is close to the momentum of the projectiles, was quite effective for measurements of hypernuclei lifetimes and production cross sections. The dedicated and very selective trigger on two body hypernuclei decays with negative pion was the key point of this approach. As a result, the accuracy of lifetime measurements was, therefore, restricted mainly by statistical errors. The values of the experimental cross section were in good agreement with the results of the calculations [7] (see also the review [8]) performed using the coalescence model. It should be noted that hypernucleus lifetime up to now remains an actual problem.

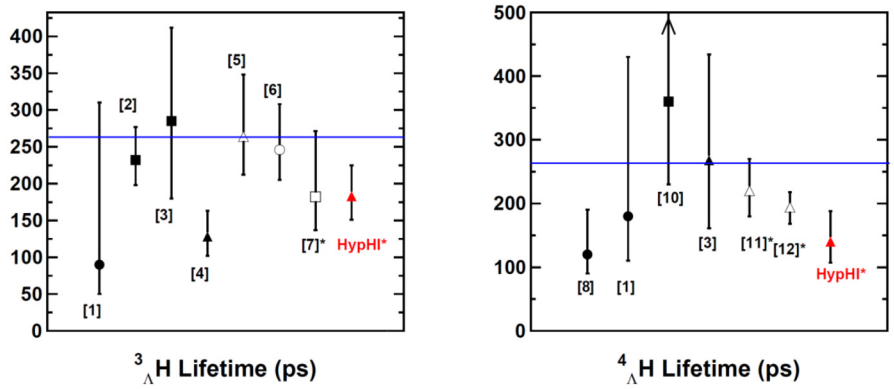

Figure 1: World data comparison of ${}^{3}_{\Lambda}$H and ${}^{4}_{\Lambda}$H lifetimes presented by Rappold in Proceedings [10] where references are listed. It should be said that ${}^{4}_{\Lambda}$H lifetime value noted as [11] is result of our previous experiment [20]. Values obtained in the HypHI experiment [10], are indicated as "HypHI". The horizontal line at 263.2 ps shows the known lifetime of the Λ hyperon.

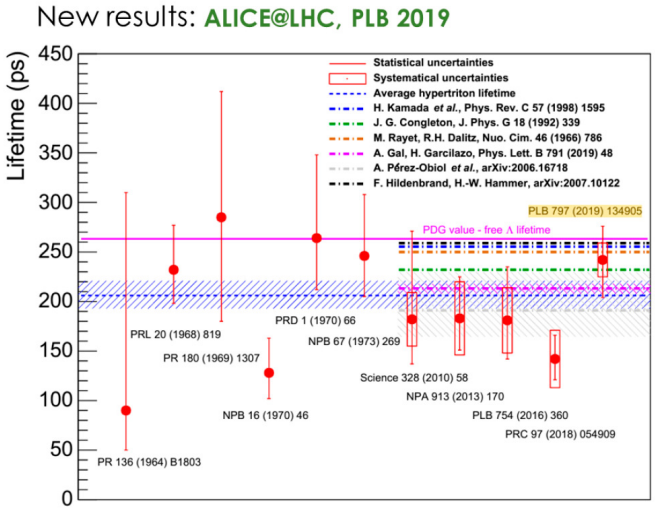

Figure 2: The summary of hypertritium lifetime measurement value in the period from 1964 till 2022. The data are taken from A. Ramos presentation at Hyp2022 in Prague [13].

In all previous hypernuclear experiments except the above mentioned Dubna experiments [17] and the Heavy Ion Beam experiment at GSI, Darmstadt [18, 19], hypernuclei are produced in various

processes of a target excitation. The common feature of all such experiments is that momentum of the produced hypernucleus is low and the last decays practically at the production point inside the target. On the contrary, in Dubna experiments, the energy of hypernuclei is only slightly lower than that of the beam nuclei, see Fig. 3. Therefore, the hypernucleus lifetime in the laboratory reference frame is increased by the Lorentz factor $3-7$ and a significant part of hypernuclei decays far behind the production target. Thus, the location of the decay vertices can be used for identification of a hypernucleus decay and for determination of the lifetime of the observed hypernuclei by measurements of their decay path distribution. In other words, the lifetime "is converted" into the flight path which could be unambiguously measured with a good accuracy.

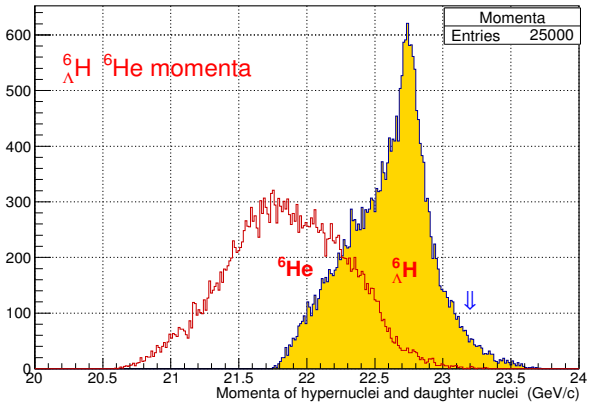

Figure 3: Expected distributions of momenta of $^{6}_{\Lambda}$H hypernuclei and the daughter nuclei, ^{6}He, are shown. The beam momentum, 23.2 GeV/c, is indicated by the arrow. Due to Fermi motion and beam fragmentation, momenta of few hypernuclei are higher than the mean momentum value for 6 nucleons (^{7}Li beam).

The HyperNIS program is focused on properties of hypernuclei with a neutron rich halo. In the last time, properties of neutron rich hypernuclei and double hypernuclei are highly anticipated to revise the theory of neutron stars to solve the hyperon puzzle. The distribution of the baryon chemical potential in neutron stars predicts that a part of baryons should be Lambda particles but inclusion of Lambdas can change most of temporary suggestions for the equation of state (EoS) so that $1.4-1.5$ solar masses would be a limit of the neutron star mass while it is known that masses of two of them are equal to two solar masses [21]. Recently, the theory suggests how to solve the problem [22] but new hypernuclear experimental data will help to choose the proper way.

First of all, the study of $^{6}_{\Lambda}$H hypernucleus will be carried out with the ^{7}Li beam:

$$^{7}\mathrm{Li} + C \rightarrow ^{A}_{\Lambda}\mathrm{H} + \mathrm{p(d,t,n)} + \ldots \rightarrow ^{A}\mathrm{He} + \pi^{-} + \ldots \quad \text{where A=3, 4, 6.} \tag{2}$$

We have chosen the ^{7}Li beam because an extra proton from ^{7}Li can be stripped by fragmentation while an additional charge exchange reaction is necessary if the ^{6}Li beam is used to produce the $^{6}_{\Lambda}$H hypernucleus. The probability of fragmentation is much higher than that of the charge exchange reaction. The double charge exchange problem considering $^{6}_{\Lambda}$H hypernucleus production is discussed, for example, by A. Sakaguchi [23].

An evidence for three $^{6}_{\Lambda}$H hypernuclei was reported from Frascati [1, 2]. On the other hand, E10 collaboration at the J-PARC experiment did not observe the missing mass peak corresponding to $^{6}_{\Lambda}$H production [4, 23], but before the J-PARC experiment A. Gal predicted that the possibility to see the $^{6}_{\Lambda}$H signal, is low in that case. A reason is that the spectrometer at J-PARC is not suited well for the task since the energy of recoil nuclei is too high while the pion beam produces hypernuclei of high excitation levels that is impossible in the case of low hypernucleus binding energy. Moreover, to produce $^{6}_{\Lambda}$H using ^{6}Li target, the double charge exchange reaction is necessary. The process is

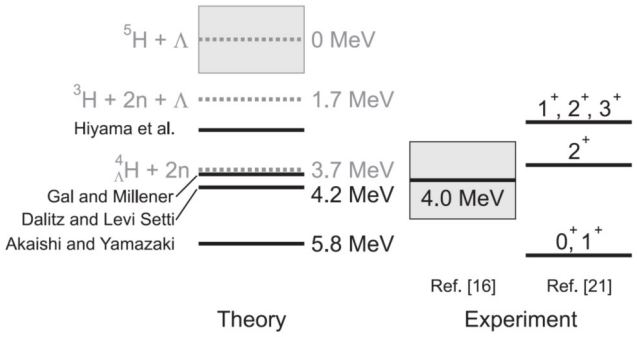

Figure 4: A summary of energy levels of $^6_Λ$H. In the left side theoretically calculated binding energies from [29, 30, 25, 24] are shown. The right side shows energy levels and binding energies reported by the FINUDA collaboration in [1, 2]. All the binding energies are measured from the ^{5}H+Λ threshold.

suppressed and a lot of uncertainties should be solved to predict the production rate. Anyway, the search of $^6_Λ$H was not a part of J-PARC research program for the period till 2030. Theoretical predictions are strongly model dependent and controversial as well. For example, E. Hiyama and others [24] have calculated that $^6_Λ$H is not a stable nucleus and should decay into $^4_Λ$H+n+n if one takes into account the parameters of ^{5}H resonance measured up to now. At the same time there are estimates [25, 26] showing that the binding energy of $^6_Λ$H should be about a few MeV. So, it is necessary to carry out an experiment that can test existence of $^6_Λ$H hypernucleus without a doubt.

At J-PARC, the search of $^6_Λ$H was the first phase of the E10 experiment which was performed at the J-PARC 50 GeV proton-synchrotron facility. However, the search of $^6_Λ$H using the ^{6}Li(π^-,K$^+$) reaction at the pion beam momentum of 1.2 GeV/c gave no events again [23].

Anyway, it seems that if pion beams are used, the $^6_Λ$H production cross section is tiny and more precise experiments will be difficult. On contrary, we suggest to use ^{7}Li fragmentation due to a much higher reaction probability instead of DCX for ^{6}Li.

At this point one should note that no hypernuclei were directly observed at Frascati and J-PARC experiments. Only secondary effects like negative pions assumed to be products of the $^6_Λ$H decay or the missing mass of the possible production reaction, were determined. Since statistics at Frascati was very low (only 3 candidates) and no signal at J-PARC was observed, the situation is controversial. Therefore, a crucial experiment can be carried out at the VBLHEP of JINR. The search of $^6_Λ$H with the HyperNIS spectrometer to obtain quite high statistics (few hundreds of detected events), should be made in order to measure the lifetime and production cross sections. That will provide a basis to solve the problem whether hyperons indeed are acting as a "glue" in the vicinity of the neutron rich drip line. Also, the mass of the isotope $^6_Λ$H can be measured with the use of our magnetic spectrometer. Actually, at the Dubna experiment, three isotopes of hydrogen hypernuclei ($^3_Λ$H, $^4_Λ$H, $^6_Λ$H) have to be produced simultaneously. It must be stressed that $^3_Λ$H and $^4_Λ$H can be used as "reference points" to confirm production and the decay of $^6_Λ$H. Sure, lifetimes of all these hypernuclear isotopes can be measured as well.

Production of hypernuclei with a large neutron excess and a neutron halo was discussed by L. Majling since 1994 [27, 28]. A possibility was pointed out to study the baryon-baryon interaction in the system with an extremely large value of $N/Z = 6$. It was also emphasized that the measurement of the $^6_Λ$H mass allows verification of the assumption that the binding energy of neutron-rich hypernuclei increases due to the specific "coherent $\Lambda - \Sigma$ mixing mechanism" [31, 32]. It should be noted that there is a chain of four nuclei with two neutron halo and different compositions of the S-shell core: with and without Λ hyperon, namely the nuclei ^{5}H, $^6_Λ$H, ^{6}He, $^7_Λ$He. Thus, the study of $^6_Λ$H properties

Table 1: Measured and estimated cross sections of hypernucleus production. The calculations are taken from [7]. For the ^{7}Li beam on the carbon target, we have measured [33] the cross section of the charge change, $\sigma_{cc} = 650 \pm 20$ mb.

Beam	Hyper- nuclei	Energy, AGeV	Cross sec., μb Theory	Exp.
^{3}He	$^3_\Lambda$H	5.14	0.03	$0.05^{+0.05}_{-0.02}$
^{4}He	$^3_\Lambda$H	3.7	0.06	< 0.1
	$^4_\Lambda$H	2.2	0.08	< 0.08
		3.7	0.29	$0.4^{+0.4}_{-0.2}$
^{6}Li	$^3_\Lambda$H	3.7	0.09	$0.2^{+0.3}_{-0.15}$
	$^4_\Lambda$H	3.7	0.2	$0.3^{+0.3}_{-0.15}$
^{7}Li	$^7_\Lambda$Li	3.0	0.11	< 1
	$^6_\Lambda$He	3.0	0.25	< 0.5

as well as those of $^6_\Lambda$He, will be significant for the theory. Also it was noted that existence of the $^8_\Lambda$H hypernucleus might be possible. If the first experiment with $^6_\Lambda$H will be successful, the following search of $^8_\Lambda$H hypernucleus is the most natural aim. We propose to use the ^{9}Li beam for such the experiment. Also let us note that the search for $^8_\Lambda$H using pion or kaon beams is even more difficult than the study of $^6_\Lambda$H. The ^{9}Li beam will be created as a secondary beam when carbon is accelerated one. Lifetimes of ^{9}Li and ^{8}He are of the order of hundred milliseconds that is long enough for the experiment. The chain of possible processes is

$$^{12}\mathrm{C} + \mathrm{Al} \rightarrow ^9\mathrm{Li} + \mathrm{C} + \ldots, \quad ^9\mathrm{Li} \rightarrow ^8_\Lambda\mathrm{H} + \mathrm{p} \rightarrow ^8\mathrm{He} + \pi^- + \mathrm{p}.$$

Expected production cross sections of the lightest hypernuclei are given in Table 1. New data from the present project will significantly improve the description of the hypernucleus production process. Taking into account values from the table we have estimated the possible counting rate of $^4_\Lambda$H pionic decays equal to 600 events per day in the case of ideal Nuclotron operation conditions (the spill length is 5 s, there are no intensity pulsations, etc.). However, real tests have shown that this value should be reduced few times to $150 - 200$ events per day. If we suppose that the binding energy of $^6_\Lambda$H is low, we can expect that its production cross section is of the same order as for $^3_\Lambda$H. Then, one can expect to register $30 - 40$ events of $^6_\Lambda$H per day. But we should underline that all estimates are based on the idea that coalescence is similar in all hydrogen hypernuclei production processes.

At the next stage of the experiment, the $^6_\Lambda$He hypernucleus will be investigated with the ^{6}Li beam. $^6_\Lambda$He will be produced in peripheral interactions of lithium with the carbon target and the trigger will be tuned in order to select pionic decays producing the negative pion and the daughter lithium nucleus emitted from the decay region:

$$^6\mathrm{Li} + \mathrm{C} \rightarrow ^6_\Lambda\mathrm{He} + \ldots \rightarrow ^6\mathrm{Li} + \pi^- + \ldots \tag{3}$$

It was established that $^6_\Lambda$He hypernucleus is loosely bound (the neutron separation energy, $B = 0.17 \pm 0.10$ MeV). But its lifetime and production cross section were not measured up to now. The measurement of the $^6_\Lambda$He lifetime is the first task of the $^6_\Lambda$He experiment. While $^5_\Lambda$He hypernuclei are investigated very well, the study of $^6_\Lambda$He was stopped after emulsion experiments since it is not so easy to produce $^6_\Lambda$He hypernuclei in other experiments due to weakly bound neutron within it. Meanwhile, $^5_\Lambda$He is easily produced in kaon or pion beams if a ^{6}Li target is used.

The method of Coulomb dissociation suggested in [20, 34, 35, 36], will be exploited for the experimental estimation of ${}^{3}_{\Lambda}$H and ${}^{6}_{\Lambda}$He binding energies. This method is interesting from the experimental point of view because interactions of hypernucleus "beam" should be investigated.

More complicated experimental skill and instruments should be used for the next stage of research tasks devoted to the study of nonmesonic decays of hypernuclei. It is well known that removing one neutron from ^{9}Be results in ^{8}Be* with the subsequent double α-decay. Due to this salient feature of the core of nuclei ^{9}Be and ^{9}B, it may be possible to identify final states of the residual nucleus. In the experiment, one should register a chain of decays, for example, ${}^{10}_{\Lambda}$B which decays as ${}^{10}_{\Lambda}$B $\rightarrow n + p +$ ^{8}Be* with the subsequent ^{8}Be* decay emitting two α's within a very small angle. We are going to experimentally determine branching ratios $\Gamma^{n\,(p)}_{\alpha\alpha\,i}$ for exclusive decays of ${}^{10}_{\Lambda}$Be and ${}^{10}_{\Lambda}$B hypernuclei. This task can be made during SRC run at HyperNIS setup with the carbon beam.

The energy of the α-particles determines the final state of the residual nucleus ^{8}Be, i.e., its quantum numbers and hence also the actual weight of the four possible wave functions of the NΛ-pair: $p_{\frac{1}{2}}s_{\Lambda}$ with J = 0, 1 and $p_{\frac{3}{2}}s_{\Lambda}$ with J = 1, 2. The branching ratios $\Gamma^{n\,(p)}_{\alpha\alpha\,i}$ depend on various combinations of four matrix elements $w^{SJ}_{\ell\tau}$. As a result, their study offers a unique possibility for determination of all needed matrix elements of the weak interaction [17, 37]. The knowledge of these $w^{SJ}_{\ell\tau}$ will open a possibility to extend the phenomenological model of Block & Dalitz [38] up to p-shell hypernuclei.

Because the two alpha particles and the decay products of the excited hypernuclei are emitted in a very narrow cone, additional high resolution detectors should be installed to detect twin alpha particles. Calculations have shown that gas electron multiplier (GEM) detectors with the 10×10 cm^2 area can solve the problem. An additional trigger counter with a thin (1 mm) quartz radiator can suppress in 30-50 times the background coming from the beam nuclei fragmentation in the trigger detectors.

Spectrometer scheme

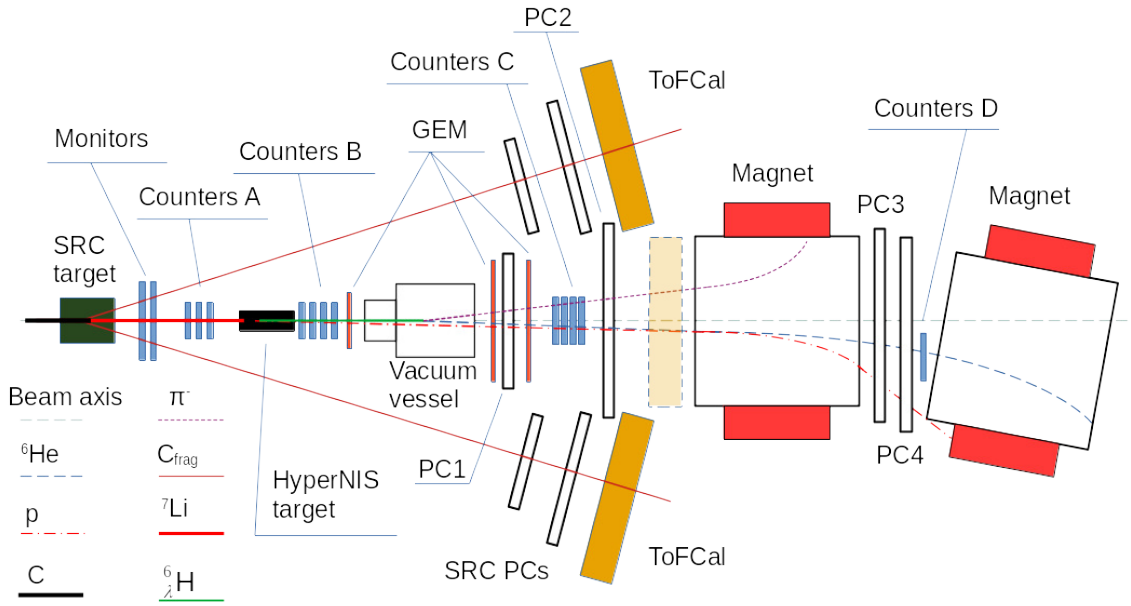

Figure 5: The configuration of the HyperNIS+SRC spectrometer is presented in particular, for the search of ${}^{6}_{\Lambda}$H hypernuclei with the ^{7}Li beam (not in scale). The scheme contains: the HyperNIS target; beam monitor counters; groups of trigger counters A, B, and C; the vacuum decay vessel of 55 cm length; 4 groups of proportional chambers PC1–PC4; the ToFCal station which should be installed in front of the first magnet (the faded rectangular on the scheme); two analyzing magnets with the magnetic field 0.6T (only one is used for this configuration); the scintillation counter D which confirms the registration of ^{6}He nuclei, i.e., detects that a daughter nucleus is not ^{3}H but ^{6}He. The HyperNIS carbon target has sizes $12 \times 3 \times 3$ cm and the density 20.4 g/cm^2.

The configuration of the spectrometer is presented in Fig. 5. The carbon target is placed at 12 cm

along the beam and has the cross section 3×3 cm^2 and the density 20.4 g/cm^2. When hyperhydrogen ($^3_\Lambda$H or $^4_\Lambda$H or $^6_\Lambda$H) is produced in interactions of the ^{7}Li beam nuclei with the carbon target, the pionic decay

$$^A_\Lambda\mathrm{H} \rightarrow {}^A\mathrm{He} + \pi^- \quad (A = 3, 4, 6) \tag{4}$$

will occur inside the vacuum vessel with a rather high probability. The Cherenkov and scintillation counters (the trigger detectors B and C, correspondingly) are tuned to measure the charge difference between hypernucleus and its decay products. Taking into account that the resolution of a Cherenkov counter is better than scintillation one, a block of four Cherenkov counters is used as B detector as discussed above. Blocks of proportional chambers PC1 (four chambers 38×38 cm^2) and PC2 (two chambers 130×80 cm^2) register hits from pion and the daughter He nucleus, allowing the reconstruction of the decay vertex. In addition, the set of all the proportional chambers, PC1–PC4, is used to measure the momentum of the He nucleus. The chambers PC3 and PC4 are of the same size as the chambers PC2. The full set of the chambers allows to detect the secondary proton or another ^{7}Li fragment and to separate the momentum of the daughter nucleus produced in the decay of the hydrogen hypernucleus, i.e., a helium isotope. The scintillation counters D are used to measure and to record the signal amplitude to separate ^{6}He daughter nuclei from tritium fragments produced together with $^4_\Lambda$H hypernuclei.

Experimental method

We would like to underline six main features of the method elaborated at JINR:

1. It is based on the idea to investigate a high energy hypernucleus produced due to a beam nucleus excitation.
2. Such hypernucleus decays occur outside the target that allows one to organize a selective trigger and to identify produced isotopes separating daughter nucleus momenta.
3. The trigger is tuned to find pionic decays of hypernuclei when the charge of the daughter nucleus is higher than that of the hypernucleus and no physical event can simulate the such charge (and, consequently, the counter signal) relation.
4. Decay products are forwardly collimated. Therefore, the spectrometer acceptance is high.
5. We analyze events when the hypernucleus decay vertex is observed in vacuum where no background interaction can simulate the decay.
6. Momenta of different hypernucleus isotopes are separated by large gaps (like momenta of daughter nuclei which are measured by the spectrometer) and therefore, it is easy to identify isotopes ^{3}He, ^{4}He, and ^{6}He.

Calculation of the momentum distributions shows that ^{3}He, ^{4}He, and ^{6}He fragments from the reaction (1), even in the case of large possible errors of momentum measurements, for example, 2%, are clearly separated. In order to measure momenta of relatively slow pions emitted at quite large angles, the time-of-flight method will be used. For this purpose, ToFCal walls should be moved to the magnet entrance so that due to the 12 cm wide gap they do not distort helium momenta. The ToF system will be used to determine masses of hypernuclei. The decay vertices can be found safely if the decay opening angle is not too narrow. We estimate the efficiency of vertex reconstruction at a level of 90% since opening angles are concentrated at higher values, see Fig. 7.

In 2022 two GEM detectors of 40×40 cm size were produced at CERN. They can reduce the number of events rejected due to the narrow opening angle (see below) and to increase the accuracy of location of the hypernucleus decay point. As a result, the tracking efficiency will be improved as well. Monte-Carlo (MC) calculations have been performed to choose optimal geometry of the target and

proportional chambers. We should remind that decay products, i.e. pions and daughter nuclei, are forward collimated so that we can find chamber positions to register more than 90% of decay pions. Certainly, all daughter nuclei hit proportional chambers.

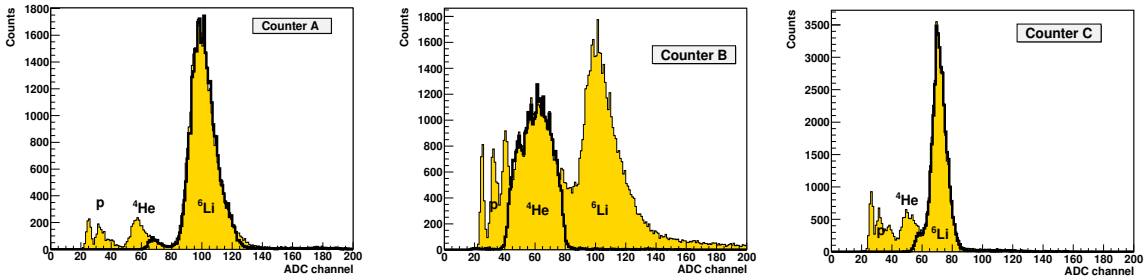

Figure 6: Tuning of trigger (scintillation) counters with the ^{6}Li beam for $^6_\Lambda$He production and the decay. Examples of spectra of the signal amplitude obtained for counters A, B, and C, correspondingly, are shown. Peaks of the signal amplitude correspond to the lithium beam and its fragments from interactions with the Al target inserted into the beam to produce different lithium fragments i.e., helium and hydrogen isotopes. The part of spectrum discriminated by thick line contours, is determined by counter discriminators which are tuned to register lithium for counters A and C and helium for the counters B. As it was mentioned, scintillation counters B were replaced with Cherenkov counters.

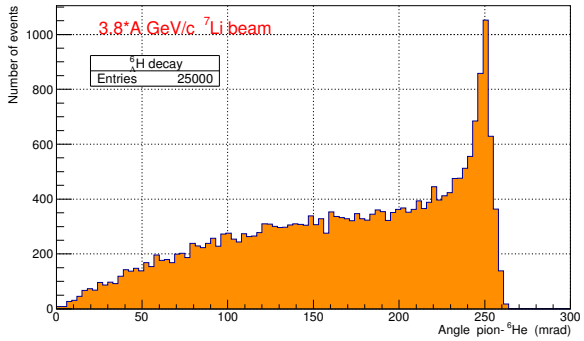

Figure 7: The distribution of the calculated pion helium separation angle for $^6_\Lambda$H$\rightarrow \pi^- + ^6$He decays is shown. About 10-16% decays have separation angles below resolution of the proportional chambers but can be detected using GEM detectors in future experiments.

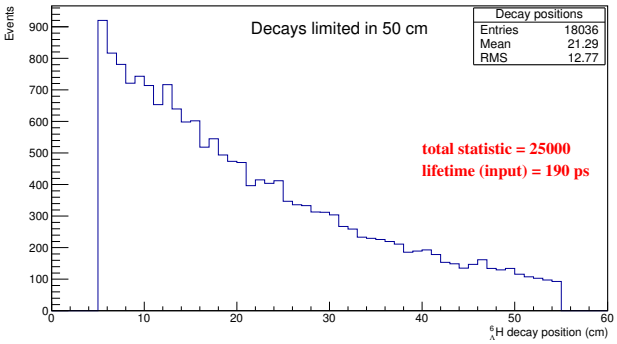

Figure 8: Expected decay points inside of the 50 cm decay volume are plotted. Since 25000 events were analyzed and about 18000 decays of hypernuclei were found inside of the 50 cm distance, we obtain the probability of approximately 70% that the first point is at the distance of 5 cm from the target.

A trigger was developed for detection of pionic decays of hypernuclei. It was used successfully in the previous experiment in Dubna [5, 6, 17]. The idea of the trigger is as follows. When the $^6_\Lambda$H hypernucleus is produced, the ^{7}Li nucleus has to emit a spectator proton while the remaining core, the ^{6}He nucleus, is transmuted into $^6_\Lambda$H. Each of these two particles has the charge equal to 1 (total $Z = 1+1$) and hits the block of the Cherenkov counters B. Since the counter response is proportional to Z^2 of the interacting particle, both particles will create in the Cherenkov counters B signals proportional to the sum of charge squares, $U = 1^2 + 1^2 = 2$. As performed MC calculations show, less than 2-3% of recoil protons or slow associated K^+ hit Cherenkov counters B which are insensitive to slow particles.

The mesonic decay $^6_\Lambda$H$\rightarrow ^6$He$+\pi^-$ produces particles with $Z = 2$ (He) and $Z = -1$ (π^-). The scintillation counters C of a minimal size are used in order to register mainly the daughter helium nuclei. Most pions will miss these counters and such the condition provides the best amplitude resolution of counters C. It is also expected that a significant fraction of the spectator protons will hit the counters. However, it is desirable to have a trigger working at the full capacity and therefore, one should ensure that the trigger works efficiently when the counters C have a signal proportional to $U = 2^2 = 4$ for the case when only helium hits the counters C, $U = 2^2 + 1^2 = 5$ when proton or pion also hit the counters, and $U = 2^2 + 1^2 + 1^2 = 6$ when all particles hit. So, the counters C should produce a signal proportional to $U \geq 4$ *if a hydrogen hypernucleus decay takes place* but less

than $U = 9$ created by Li beam nuclei. Finally, let us underline that for the case of pionic decays, the signal registered in the counters C is higher than one obtained in the set B while for majority of background events the situation is opposite. Counters SciHe, see Fig. 5, are not a part of the trigger. Their signals are recorded and are used to check that helium-6 registered in chambers PC3 and PC4 is not background tritium. Some results of trigger tests were presented in [39, 40].

As was noted above, a significant part of hypernuclei decays straight off after the target. For example, if we assume the lifetime of the ${}^{6}_{\Lambda}$H hypernucleus equal to 190 ps, then the ^{7}Li beam with the momentum[1] 27 GeV/c produces hypernuclei with the lifetime at the laboratory frame about 760 ps due to the Lorentz factor. As shown in Fig. 8, the mentioned physical effect provides a possibility to expect 70% of hypernuclei decays inside of our vacuum vessel if it is placed at the distance of 5 cm from the target.

In order to optimize the efficiency, one should check if the short distance between the target and the vacuumed decay volume does not cause additional losses due to a narrow angle between momenta of pion and helium which is the hypernucleus daughter nucleus. Estimates show that the possible shortest distance between the target and the decay volume is the best choice. By increasing this distance we loose statistics not only due to early decays but also for the reason that pions miss the acceptance of the proportional chambers while losses due to a narrow separation angle stay in 10-16% interval and therefore, are less significant. The distribution of the He-π separation angle for the case of ${}^{6}_{\Lambda}$H decays is presented in Fig. 7. Some results of the calculated pion distribution at proportional chambers are shown in Figs. 9 and 10.

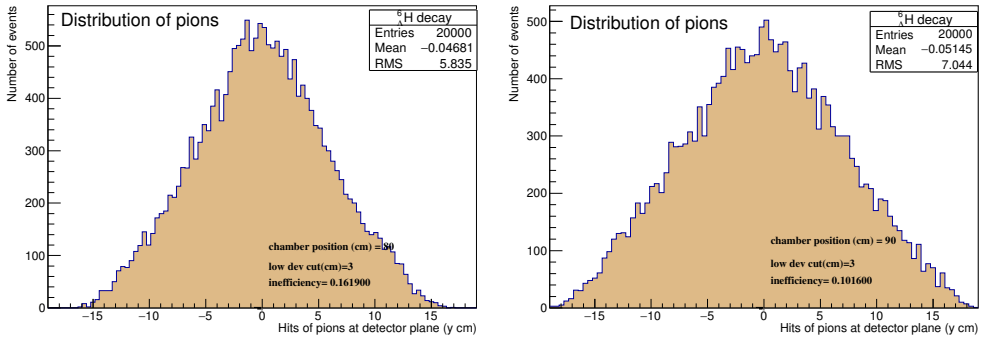

Figure 9: We demonstrate the distribution of pion hits in a proportional chamber situated at distances 80 cm (left panel) or 90 cm (right panel) from the beam entrance point of the target. There are no decay pions outside the chamber. For example, an arbitrary quite large value of the minimal distance between He and pion hits is chosen equal to 3 cm as a limit of inefficiency. The cut in the real experiment will be optimized.

Results obtained in the last years

During the Nuclotron run 50 the ^{7}Li beam was delivered to the spectrometer for the first time. The provided beam time was used mostly for tests and tuning of the modernized trigger system in the new counting room located at the new place in the experimental hall. The background suppression factor much higher than 10^4, was reached.

Recently the tracking software was upgraded and became more effective. Some results of tests with MC generated events are presented in Figs. 11 and 12.

In the last years the Nuclotron upgrade was a task of highest priority for the laboratory. We were waiting when the energy of the extracted nuclear beam will exceed the hypernucleus production threshold on such the value which allows to carry out hypernuclear experiments. During this time the deuteron beam was used for short test runs in order to calibrate the spectrometer and to test the

[1]The highest value available at the beam line is 3.8 GeV/c per nucleon.

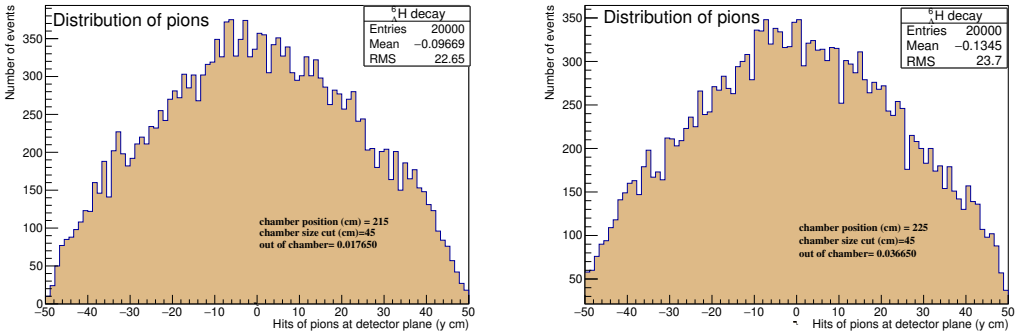

Figure 10: Pion hits at the last chamber which pions traverse, are shown. The geometrical efficiency depends the shift of the target position. The shift on 10 cm results in few percent loss as we see confronting left and right panels. For the experiment, the distance of 215 cm is chosen.

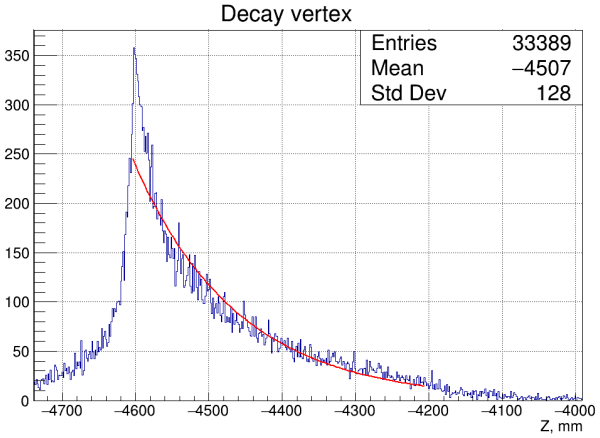

Figure 11: Properly reconstructed decay points allow one to measure the lifetime of a hypernucleus. The left edge of the fiducial decay volume is at $Z = -4600$ mm.

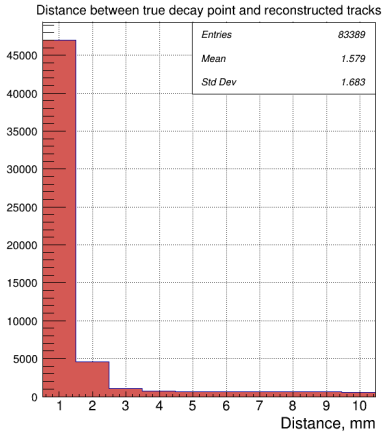

Figure 12: Decay points can be localized into 2 mm.

new equipment. Data for alignment of proportional chambers were taken, few software applications for alignment were developed and investigated, and all necessary calculations and fits were performed. Some results are presented in Fig. 13.

At the present time the kinetic energy of the extracted nuclear beam is increased up to 4 AGeV that is essentially higher than the hypernucleus production threshold. Also the beam line to the HyperNIS spectrometer was tested and the necessary nuclear beam was transported to the spectrometer. Unfortunately, in 2017-2022 the Li beam was available only for a short (63 hours) test run which was used to tune the trigger for hypernucleus detection and to test chambers. The duration of this run was too short for data taking.

On the other hand, the spectrometer was significantly upgraded during the last years. For example, a new electronic gas supply system allows one to stabilize the performance of proportional chambers.

But the most important improvement was taken place in R&D and production of 200 new front-end analog signal electronic cards of 32 channels for proportional chambers were produced in Minsk. The digital part of the FEE cards, see Figs. 14, was designed and tested in JINR.

Electronic modules of the trigger system were replaced with new ones too. All modules in VME crate, i.e., time charge digital converter (TQDC), data acquisition (DAQ), and service modules, and the main DAQ server are new. It should be underline that a new universal amplitude digitizer, DT5560S 32 Ch. 14 bit 125 MS/s, was bought and software tests was started. The usage of DT5560S allows us to remove the large amount of cable connections and provides a possibility to write signal amplitudes and times of all counters of the trigger system. As a result, we will make thresholds of the preliminary hardware trigger softer to use the digital final software trigger later and to select hypernuclear events

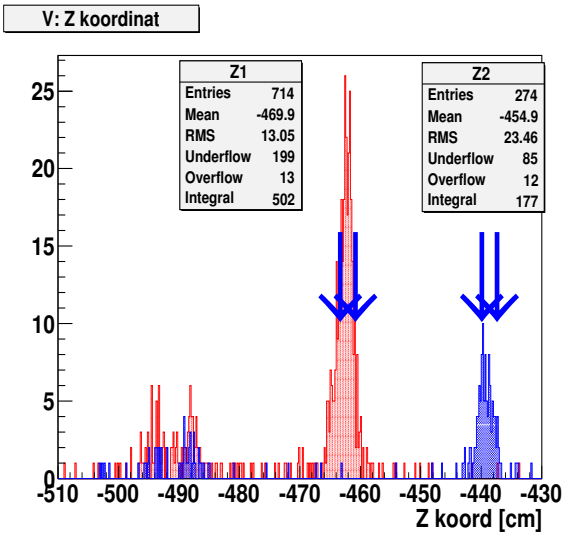

Figure 13: Positions of reconstructed ${}^{6}_{\Lambda}$H along the beam axis are plotted. The results of a test of alignment codes and vertex reconstruction procedure are presented. The target was placed at two positions (red and blue histograms). The arrows show the edges of the target. The position of two monitor trigger counters is also seen. The vertex position is the point of the minimal distance between two tracks ($d < 2$ mm).

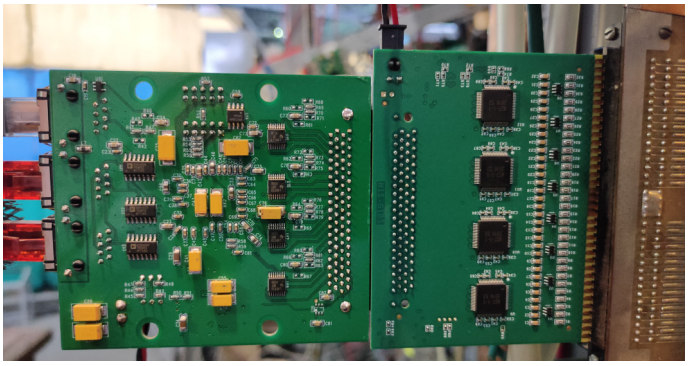

Figure 14: The FEE cards are shown. The left plate is the digital part for data processing and transfer. The right plate is the the analog signal amplifier part where one can see chamber output contacts.

more carefully. Systems of on-line service as the beam control, monitoring of the chamber efficiencies, the slow control for high voltage supply units, and others, were elaborated, tested, and are used. Since the beam intensity in the hypernuclear experiments is relatively low, $10^5 - 10^6 s^{-1}$, it is necessary to organize the Internet access to the beam control data for the Nuclotron staff. Moreover, taking into account experience of test runs, this system is upgraded from run to run. All data from trigger counters are available in the Nuclotron control room and can be used by the staff to improve beam tuning.

A new high voltage supply system was put into operation for trigger photomultiplier tubes. It has up to 64 very stable outputs driven by WIENER MPOD crate controller. The corresponding programs was adapted by HyperNIS members. The proportional chambers are driven using CAEN high voltage supply modules. In time, low voltage systems for proportional chambers were obtained and installed as well. Recently, a block of four Cherenkov trigger counters was produced. The carbon target is situated inside of the block closely to quartz radiators in order to minimize losses of observed hypernuclei due to decays[2]. The produced Cherenkov block was tested and the amplitude resolution was obtained higher than in the caseof the scintillation counter block, see Figs. 15 and 16.

To reject the possible background of nuclear fragments produced in the trigger counters, primarily

[2]Approximately 20% of hypernuclei decay at very first five centimeters after the target.

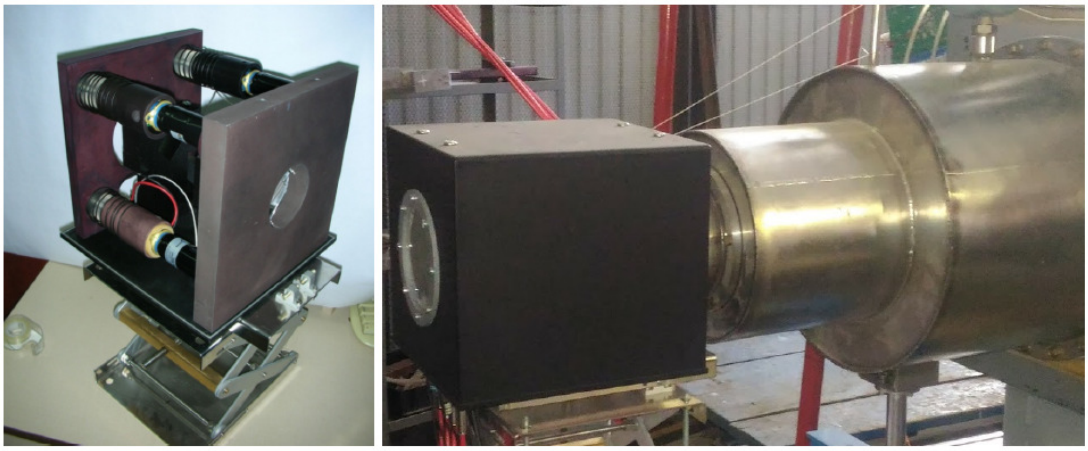

Figure 15: The block of four Cherenkov counters with four subsequent quartz radiators each of the 4 mm thick, is demonstrated. On the left side, one can see three of four Electron Tubes 9107B photomultipliers. The high density graphite (1.7 g/cm^3) target is placed closely to radiators. The block itself is placed near the vacuum vessel as you can see on the right side of the figure.

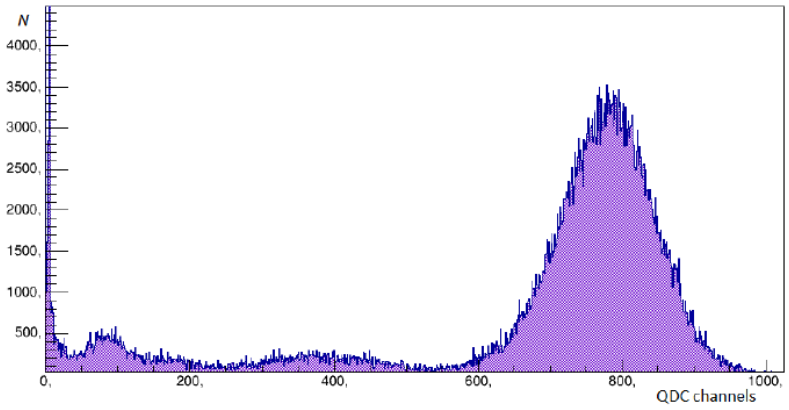

Figure 16: The pulse height distribution of lithium fragments measured with one of the Cherenkov counters. A clean separation is obtained for hydrogen, helium, and lithium.

tritium, several additional scintillation counters (the set D) were produced and tested.

Plan for the coming years

Taking into account that two different experiments are proposed, first one with the ^{7}Li beam and the second with the carbon beam, one should carefully plan the change of beams and tasks. For the hypernuclear experiment, the optimal schedule can be like that below:

- The focus will be made on the hypernuclear program of the HyperNIS project with the use of the d and ^{7}Li beams (the deuteron beam is needed for methodical purposes). In the first and second years two GEM detectors will be installed to improve the decay vertex localization.
- The study of the hypernucleus ${}^{6}_{\Lambda}$H in the first and second years: the search of ${}^{6}_{\Lambda}$H with subsequent measurements of the lifetime with the accuracy of $10-15$ ps, the production cross section, and the mass with accuracy of $1-2$ MeV if the isotope exists. Minimal necessary statistics for these goals is about 500 detected events of ${}^{6}_{\Lambda}$H production. If the production cross section is as low as in the case of ${}^{3}_{\Lambda}$H, approximately two hundred hours of the lithium beam are necessary.
  If the first ${}^{6}_{\Lambda}$H experiment is successful, we will continue to take 2000 detected events of ${}^{6}_{\Lambda}$H production to check predictions of two lifetimes of ${}^{6}_{\Lambda}$H isomeric states or to search for the ${}^{8}_{\Lambda}$H hypernucleus using the ^{9}Li beam. The last task is preferable.
- In the first two years the technical design and mounting which are necessary for SRC detectors and the additional magnet, will be performed.

- In the third year the study of poorly investigated ${}^{6}_{\Lambda}$He has to be made including measurements of the lifetime and the production cross section. At least 500 events of ${}^{6}_{\Lambda}$He production have to be detected.
- In the last two years we are planning the search of ${}^{8}_{\Lambda}$H hypernucleus, the study of nonmesonic decay of medium hypernuclei ${}^{10}_{\Lambda}$Be and ${}^{10}_{\Lambda}$B which requires high statistics due to rare events of production and decay of hypernuclei ${}^{10}_{\Lambda}$Be and ${}^{10}_{\Lambda}$B. Fortunately, this task can be simultaneously solved with the data collection for the SRC experiment. Also tests for the measurement of Coulomb dissociation of ${}^{3}_{\Lambda}$H can be made.

The first stage of the research program of the HyperNIS project has to be finished in four years. The most important technical result of the project is that a new multipurpose magnetic spectrometer with modern detectors and electronics will be commissioned and will be ready for hypernuclear experiments using extracted Nuclotron beams. The spectrometer will be also available for other experiments, e.g., tests of detectors and so on.

Present status of the apparatus.

After test runs at the Nuclotron beam, the HyperNIS spectrometer is commissioned. The extracted beams of deuteron, ^{6}Li, and ^{7}Li with the kinetic energy of $1.0 - 3.5$ GeV/nucleon and the intensity of $10^4 - 10^5$ s^{-1} were used in the test runs.

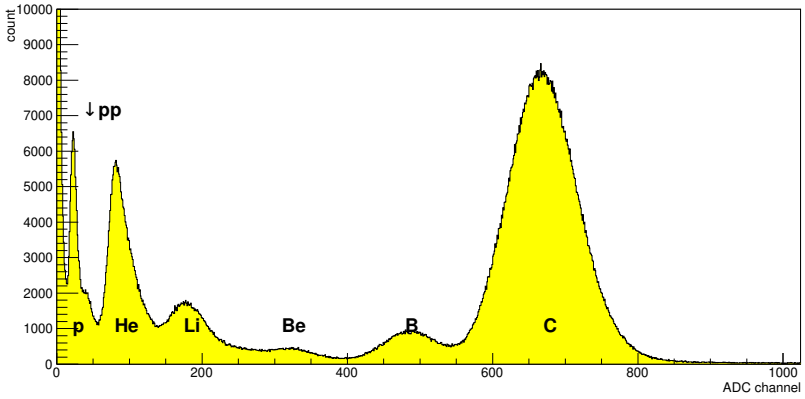

Figure 17: Amplitudes of carbon fragments measured for the carbon beam at the Al target are shown for a trigger scintillation counter.

To provide particles with different electric charges for the trigger tests, the ^{6}Li beam passed through the aluminium target. The composition of the resulted beam after the target is shown in Fig. 6. Similarly, the resolution of the counters and that the counter response is directly proportional to the ionization were tested with the carbon beam, see an example of the signal amplitude spectrum for carbon and its fragments in Fig. 17.

It should be noted again that trigger electronics was upgraded in the last few years. Any possibility to have a beam, was used to test the trigger for the study of hypernuclei even if the beam was not suitable for hypernuclear experiments. While early tests give the background suppression of the order of $2.5 \cdot 10^3$, see, for example, [40], the background rejection of the order of 10^4 was achieved in the test run with the ^{7}Li beam. We would like to underline that we use two triggers simultaneously. One of them is aimed to search for production and decays of hypernuclei while the second is included to check that the spectrometer performance is good. Since the rate of the hypernucleus trigger is low, the second trigger was tuned to detect events every 100 ms when a minimum ionizing particle (MIP) particle crosses counters and proportional chambers. This trigger is used for checking efficiency of all chambers and for the on-line control in the analysis of systematic errors.

The hypernucleus trigger selects if the such sequential change of the charge, $U = 3 \to U = 2 \to 4 \leq$

$U < 9$, is found. The trigger generates the signal for the reaction

$$^7\mathrm{Li} + \mathrm{C} \rightarrow {}^A_\Lambda\mathrm{H} + \mathrm{p(d,t,n)} + \ldots \rightarrow {}^A\mathrm{He} + \pi^- + \mathrm{p(d,t,n)} + \ldots, \quad A = 3, 4, 6.$$

A test run was carried out with the renovated trigger system situated in the new counting room and for the ^{7}Li beam with the high energy, 3 AGeV. This run showed that the trigger can be tuned to suppress the background by a factor much higher than 10^4 [41].

The production of GEM detectors was completed but they have not been delivered to Dubna yet due to logistical difficulties. An advantage of the GEM is that readout electronics is similar to one used at LHEP experiments and can be integrated into our DAQ system. This detector improves the algorithm for the search of a hypernucleus decay vertex. If GEM is installed between the trigger block B and vacuum and registers three particles, we reject the event because all tree particles are emitted from the target and do not originate from a decay in vacuum. It was proposed to install two modern GEMs produced at CERN, at the HyperNIS spectrometer. These detectors, GEM1 and GEM2, will have dimensions of the active area 400×400 mm and the distance 0.5 mm between strips. We are going to install GEM1 before the first block of proportional chambers and GEM2 behind it. The space resolution of both GEMs will be near 400 μm which allows to increase the angular accuracy for tracks in two times. Furthermore, using these detectors will enlarge useful statistics by 10% since nearly 15% of events contain tracks within a narrow cone and can not be distinguished in the first MWPC. Inclusion of GEMs also results in that localization of decay vertices and, consequently, the accuracy of lifetime measurements will be improved.

Conclusions

The study of properties of lightest hypernuclei is relevant, has high importance, and can be performed at JINR with beams from Nuclotron. The trigger of the HyperNIS spectrometer works with a high suppression factor and efficiency. Installing and commissioning of the new FEE allow us to significantly improve tracking efficiency and to carry out the proposed hypernuclear experiments. It can give answers to open questions in hypernuclear physics which are very hard for answering by alternative methods and approaches. At present time the HyperNIS spectrometer is tested using beta sources and cosmic muons.

It should be noted that the HyperNIS spectrometer and the beam line can easily be used to test detectors. HyperNIS test runs were used (and can be used in future) to test pixel detectors (TimePix) from IEAP, Prague, microstrip detectors for a satellite experiment, etc. TimePix tests were carried out together with Prague's team. These tests provided good experience for young Czech researchers. Also several students for JINR were trained. An upgrade of the spectrometer, tuning of new modules and counters, and test runs have shown that the HyperNIS team is ready to achieve stated aims.

SRC

1 Introduction

After the successful campaigns conducted at the BM@N experimental area in 2018 and 2022, we present here our proposal for continuing the SRC (Short-Range Correlations) studies at JINR.

The Phase I measurements will be carried out at the HyperNIS area, utilizing a polarized deuteron beam and making use of the existing equipment at JINR. Pending approval, we believe that Phase I can be completed within the next 2-3 years.

The second phase of our project, Phase II, is dedicated to exclusive SRC studies. This phase will also take place at the HyperNIS area but will require additional research and investment in terms of design and equipment, and adjustment of the experimental area for those measurements.

Both phases are part of a broader SRC program conducted by our international collaboration. This study spans various accelerator laboratories across the globe using electrons, real photons, protons, and nuclei as probes. The primary objective of this SRC study is to enhance our understanding of the nuclear many-body system and nucleon-nucleon interactions at short distances, characterized by high nuclear densities, large relative momenta, and high virtuality.

2 Measurements in 2018 and 2022

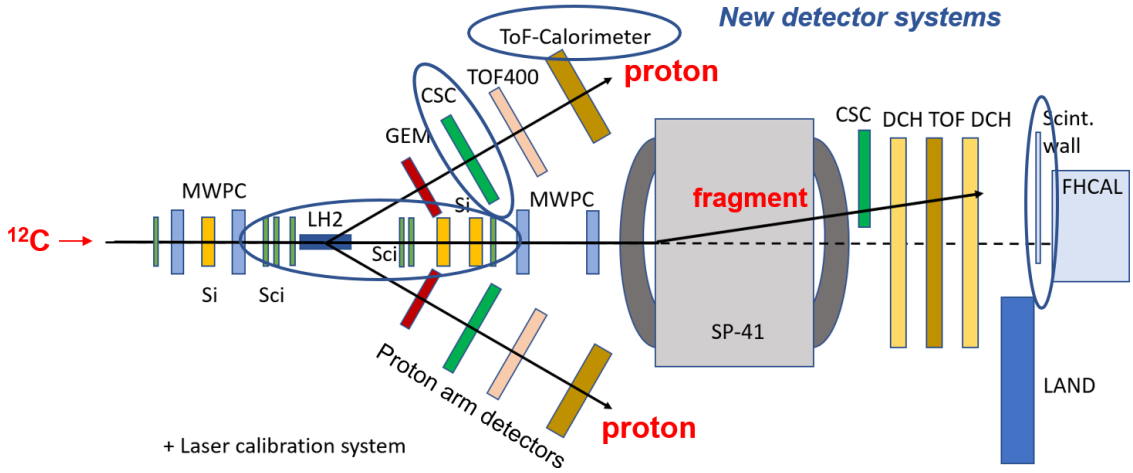

Figure 18: The BM@N spectrometer setup for the second SRC measurement in 2022. The reaction of interest is $^{12}C + p \rightarrow 2p + X$. The new detector systems added and modified after the 2018 measurement, are marked by blue ellipses.

The results of the first SRC experiment at BM@N (2018) are described in [42]. The second SRC experiment was developed to significantly enhance the statistical data by an order of magnitude. Its objectives included obtaining absolute cross-sections for quasi-free (QF) single proton removal and examining SRC pairs in carbon-12, encompassing the fragmentation of the residual A-2 system after the SRC removal. To achieve these aims, substantial improvements were made to the experimental setup, as depicted in Fig. 18. This involved the addition of a new Time-of-Flight (TOF) detector array and a set of novel scintillator trigger counters. Furthermore, a laser system was integrated to enable the simultaneous calibration of all scintillator detectors without the beam. The data acquisition

process spanned two weeks following a week-long calibration period. Presently, data analysis is in progress, and preliminary results are illustrated in Fig. 19 up to the identification of quasi-elastic events, reproducing results from the 2018 measurement on a limited data set.

Figure 2a displays the identification of incoming carbon-12 ions, while figure 2b shows the fragment spectrum. Notably, figure 2c exhibits the reconstructed reaction vertex, which clearly delineates the shape of the liquid hydrogen (LH) target. Figures 2d+e show the identification of quasi-elastic (QE) events based on proton opening angle and missing energy as reconstructed from the two-arm spectrometer. The coincidence with the 11B fragment (Fig. 2e) suppresses initial-/final-state interactions and allows to cleanly separate QE events. The corresponding missing momentum distribution is shown in Fig. 2f where, again, the fragment coincidence removes the high-momentum tail that originates from FSI effects. This reproduces our 2018 results.

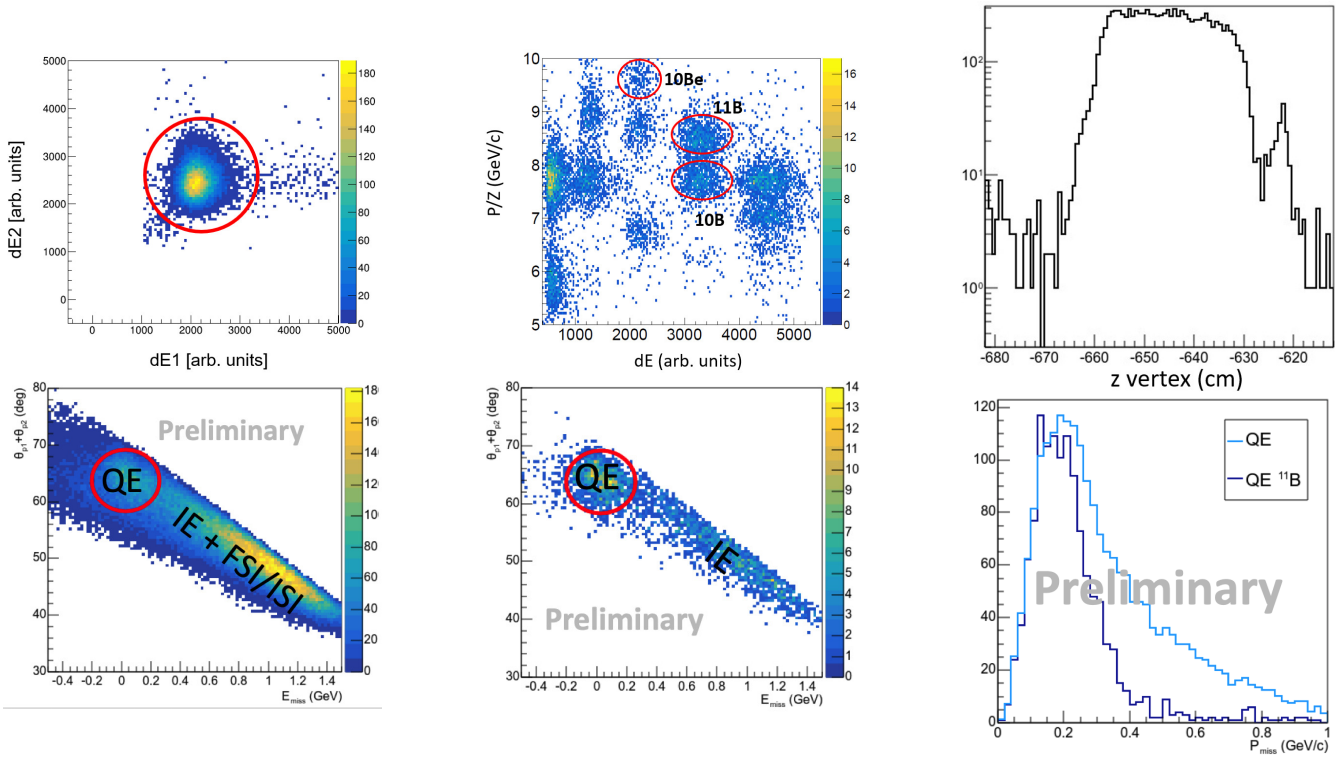

Figure 19: Preliminary results from the measurement performed in March 2022: a) identification of the incoming 12C ions using two beam scintillator counters, b) identification of the final state ion fragments, c) reconstruction of the interaction vertex coordinate along the beam using tracks in the two arms. d+e) Identification of quasi-elastic (QE) events, separating from inelastic and final-state interactions (IE, FSI), without and with 11B fragment coincidence. f) Preliminary missing momentum distribution for 12C(p,2p)11B, for a limited data set.

The dedicated SRC detectors were moved from the BM@N area and stored in the HyperNIS area in Bld. 205. The current proposal describes the continuation of the SRC program at the HyperNIS area using those detectors.

3 Polarized deuteron beam measurements in SRC kinematics

3.1 Deuterons as surrogate for two-particle correlations in nuclei

In atomic nuclei, nucleons often pair up with significant relative momenta while having small center-of-mass (CM) momenta. Here, "large" and "small" are relative to the Fermi momentum (kF) of the nucleus. These special pairs are referred to as short-range correlated (SRC) pairs [43, 44, 45]. SRC pairs provide valuable insights into several aspects of nucleon and nuclear physics, including the distribution of high momenta within nuclei, the short-distance features of the nucleon-nucleon interaction, and the inner quark-gluon structure of bound nucleons [46, 47, 48, 49, 50].

Over the past decade, we have made remarkable progress in understanding SRCs through exclusive electron hard knockout reactions, namely A(e,eN) and A(e,epN) [47, 51, 52, 53, 48], where "N" stands for a neutron or proton. These experiments were conducted on selected nuclei (A = ^{4}He, C, Al, Fe, and Pb). In these reactions, electrons interacted with protons or neutrons in the target nucleus, resulting in high-momentum transfers (QF reaction with $Q^2 > 1.5$ (GeV/c)^2). This led to the knockout of high-momentum nucleons and, in some cases, the emission of correlated recoil nucleons.

Exclusive measurements of SRC pair breakup reactions using electrons [47, 51, 52, 54, 55, 56, 45], and also protons [55, 56], on various nuclei revealed the following findings:

- Protons knocked out with high missing momentum ($300 \leq p_{miss} \leq 600$ MeV/c, where $\overrightarrow{p}_{miss} = \overrightarrow{p}_{probe} - \overrightarrow{q}$) almost always have an associated recoil nucleon with momentum that balances the missing momentum.
- These recoil nucleons are predominantly neutrons. Neutron-proton (np) SRC pairs are nearly 20 times more common than proton-proton (pp) SRC pairs, and by extension, neutron-neutron (nn) pairs. This phenomenon is termed "np-dominance," as shown in 20.
- The relative momenta of SRC nucleons within a pair, as reconstructed from the missing and recoil nucleon momenta, exceed the Fermi momentum (k_F), while the center-of-mass momenta are consistent with the total momenta of two mean-field nucleons (typically, k_F is around 250 MeV/c for medium to heavy nuclei).

From a theoretical perspective, the prevalence of np-SRC pairs over pp-SRC pairs in nuclei has been extensively examined using advanced ab-initio many-body calculations [45, 58, 59, 60, 61, 62]. These calculations underscore the dominance of np pairs at relative pair momenta greater than 300 MeV/c. By exploring various configurations of the nucleon-nucleon interaction, including the presence or absence of a substantial tensor force, we have identified the unique role of the latter in the relevant momentum range [45]. Essentially, most of the SRC pairs resemble deuteron-like states within the nucleus.

The 'Generalized Contact Formalism' (GCF) approach, as illustrated in Fig. 4, leverages the underlying dynamics of short-range correlation (SRC) pairs within nuclei [63, 64]. In this framework, the many-body wave function at short distances decomposes into two key components. First, there is a universal two-body function, which exclusively relies on the relative momentum of the pair. Second, there is a many-body function with characteristics reminiscent of a mean field, dependent on the center-of-mass momentum (p_{cm}) of the pair.

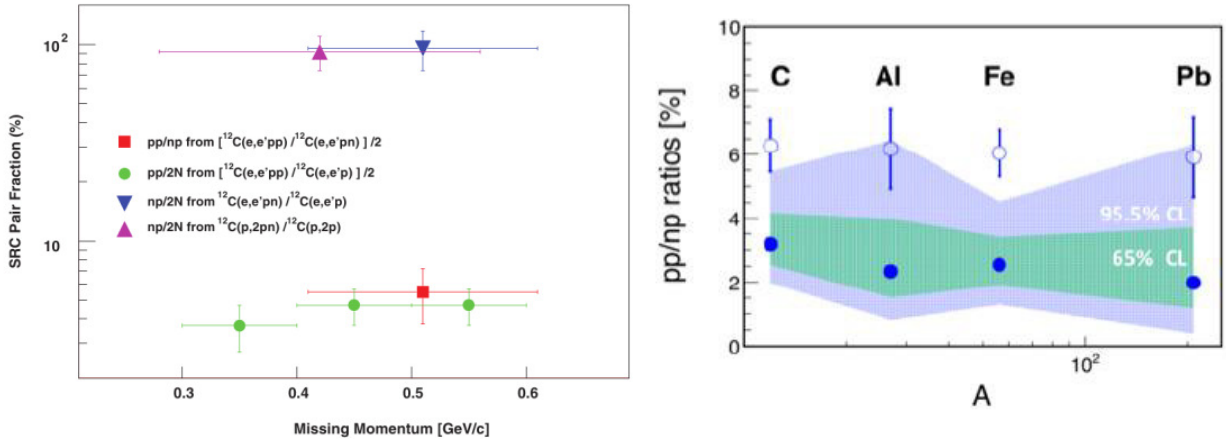

Figure 20: Results from various A(e, ep) and A(e, epN) measurements, A stands for nuclei from 4He to Pb. Left: the fraction of knocked-out protons with a correlated neutron (triangles) and proton partner (green circles), and the ratio of np- to pp-SRC pairs (red square) in C, extracted from (p, 2pn) [55, 56] and (e, epN) [47, 51, 52, 54, 55, 56] measurements; Right: the ratio of pp to pn SRC pairs for different nuclei from (e, eNp) measurements [57] without (points) and with (bands) reaction mechanism corrections. The inner and outer bands represent the 68% and 95% confidence limits of the extracted ratios, respectively.

This decomposition arises from a separation of scales within the nuclear system. There is a marked distinction between the high-momentum, short-distance scale that governs the pair relative momentum (p_{rel}), and the lower-momentum, longer-distance scale that influences the collective many-body dynamics, determining the total number of pairs and their center-of-mass momentum distribution.

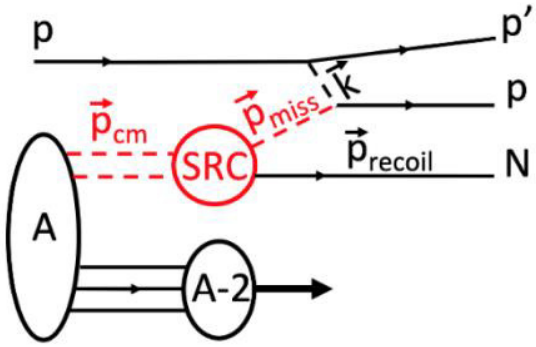

Figure 21: Diagrammatic representation and kinematics of the triple-coincidence A(p,2pN) reaction within the SRC breakup model. Dashed red lines represent off-shell particles, and the solid lines represent detected particles.

This formalism has been rigorously benchmarked against state-of-the-art VMC and Cluster-VMC calculations for nuclei ranging from ^{4}He to ^{4}0Ca, both in terms of momentum and coordinate space [65]. The results of this phenomenological approach demonstrate a high degree of agreement with ab-initio calculations, underlining its validity and utility in the study of nuclear dynamics [66, 67].

Within the GCF the A(e,e'NN) plane wave cross-section can be expressed as [63, 64, 67]:

$$\frac{d^8\sigma}{dQ^2 dx_B d\Phi_e d^3_{p_{cm}} d\Omega_{rec}} = K \times \sigma_{eN} \times n(p_{cm}) \times [\Sigma_\alpha C_\alpha \cdot |\widetilde{\phi}^\alpha(|\overrightarrow{p}_{cm} - 2\overrightarrow{p}_{rec}|)|^2], \quad (5)$$

with a similar expression for the proton scattering case. The subscripts 'N' and 'rec' stand for the leading and recoil nucleons, respectively. K is a Jacobean term, $_{eN}$ is the off-shell electron-nucleon cross-section, and α represents the quantum numbers of SRC pairs. $\widetilde{\phi}^\alpha$, $n(p_{cm})$, and C_α, respectively, describe the relative and center-of-mass motion of SRC pairs as well as their overall abundances, such that:

- $\widetilde{\phi}^{\alpha}$ are universal SRC pairs relative momentum distributions, obtained by solving the zero-energy two-body Schrödinger equation of a NN pair in quantum state α using an input NN potential model
- $n(p_{cm})$ is the SRC pair center-of-mass momentum distribution, given by a three-dimensional Gaussian with a width of 150 ± 20 MeV/c [68]
- C_{α} are nuclear contact terms that determine the relative abundance of SRC pairs in quantum state α and are obtained from analysis of ab-initio many-body calculations of two-nucleon densities. These contact terms are also consistent with the values extracted from data [65, 69, 70, 50].

3.2 Research objectives and expected scignificance

Studying nuclear structure at short distances necessitates a relativistic description of the bound system. However, there is no single prescribed method for achieving this, and the acquisition of polarization data on the deuteron is crucial for understanding the relativistic effects involved [42, 43, 71, 72, 73].

The presence of the D-wave component in the deuteron arises from the deuteron's finite quadrupole moment, which is directly associated with the tensor component of the nucleon-nucleon (NN) interaction. The tensor force does not conserve the individual spin (S) or orbital angular momentum (L) but only the total angular momentum (J). As a result, it permits a mixing of the primarily spherically symmetric S state with configurations featuring L = 2 D-state.

Modern NN interaction potentials provide predictions for the overall probability of the D-wave in the deuteron, ranging from approximately 4.87% (e.g., CDBonn) to 5.76% (e.g., AV18) [73, 74]. While this difference may appear small, these parameterizations project substantially different strengths at high momenta, particularly above 400 MeV/c, which is primarily associated with the SRC D component [75].

The knowledge of the S/D (S-wave/D-wave) ratio at large momenta is closely linked to the NN short range tensor force that is also responsible to the strong SRC np-dominance [52, 55, 66]. The S/D ratio is not an observable; however, it can be constrained within a given calculations by comparing to data. It is currently insufficiently constrained by the available data at the high momentum tail of the deuteron wave function. Proposed measurements of tensor polarization observables at SRC kinematics like the asymmetry A_{zz} [76, 77, 78, 79, 80],

$$A_{zz} = \frac{(\sigma_{-} + \sigma_{+} - 2\sigma_{0})}{\sigma_{unpolarized}} \tag{6}$$

with the yields σ for the different tensor polarization states (-, +, 0), relate in PWIA to the deuteron composition [78]:

$$A_{zz} \sim \frac{\frac{1}{2}w^2(k) - u(k)w(k)\sqrt{2}}{u^2(k) + w^2(k)}, \tag{7}$$

where $u(k)$ is the S-state wave function and $w(k)$ is the D-state wave function. This non-relativistic expression was shown to be correct also within the light front formalism by choosing appropriate value for k, see details in [80]. We propose here to collect data that is highly sensitive to the D/S ratio in the high-momentum tail as discussed below. Theoretical calculations and predictions with final-state interactions (FSI) are in progress for the proposed reaction and kinematics [79, 80, 81].

The dominant two-body SRC pairs are the neutron-proton pairs with quantum numbers of a deuteron. Measuring the polarization states in the deuteron with the unique polarized deuteron beam available at JINR is crucial for understanding SRC in nuclei. Most important advancement in this respect is the possibility of measuring polarization states at fixed and large values of internal momenta of the nucleons in the deuteron.

These studies will allow to address several questions:

- What is the deuteron wave function below the inelastic threshold?
- How do polarization states impact sensitivity to relativistic effects?
- Are there non-nucleonic components that can be observed using polarization [82]?

3.3 Rate estimations and expected uncertainties

The highest attainable beam momentum for polarized deuterons at the HyperNIS area is 6 GeV/c/nucleon, with a maximum beam intensity of 10^{10} ions per spill. We can generate various polarization modes (tensor, vector, unpolarized) by alternating the polarization for each spill. However, due to limitations imposed by our detectors and other experimental constraints, we anticipate that a realistic beam rate for data collection with our current setup would be approximately 10^6 ions per second.

Our plan involves continuing the use of the cryogenic liquid hydrogen target that was employed in the last SRC measurement at BM@N in 2022 or a similar one at the HyperNIS area. The experimental setup (as shown in Fig. 22) for studying deuteron breakup reactions necessitates a two-arm spectrometer and a downstream neutron detector along the beam. The required equipment is already available at JINR, having been utilized during the last SRC measurement period in 2022. But we will need to upgrade the electronic readout systems to meet our current research needs.

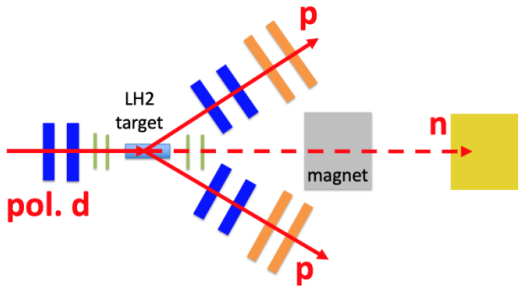

Figure 22: Schematic of the experimental setup for the studies with polarized deuteron beam. The key components are: Scintillator Beam Counters (Green): Positioned both before and after the target, these scintillator detectors serve the dual purpose of measuring the beam's start time and monitoring its charge. These detectors play a vital role in initiating and tracking the beam as it progresses through the experimental apparatus. Position sensitive Detectors (Blue): These detectors facilitate the precise reconstruction of the trajectory of the incoming beam and the protons emitted. Timing Detectors (Orange): The orange detectors are crucial for identifying the signal protons and determine their momenta. Neutron Detector (Yellow): Positioned downstream, the neutron detector is used to measure recoil neutrons.

With the incident beam rate and setup described above, we estimate that the trigger rate will be approximately 4 kHz. This estimate is based on the total proton-proton (pp) and proton-neutron (pn) cross-sections, considering a 30 cm liquid hydrogen target. Additionally, it assumes that each arm, covering about 4To estimate the rate of events relevant to the SRC study, we run realistic simulations using an event generator based on the GCF (see above) and request in the simulation-data analysis:

- $|t|$ and $|u| > 1$ GeV^2

- $60° < \theta_{cm}$
- Two-arm acceptance: $200° < \theta_{lab} < 45°$; $-20° < |\phi_{lab}| < 20°$
- $p_{miss} > 0.25$ GeV/c.

The deuteron wave function falls strongly as a function of the relative momentum between the nucleons. The obtained simulated pmiss distribution using the AV18 deuteron wave function, a data-based pp cross section parametrization, and the constraints as listed above, is shown in Fig. 23 (right). Also shown is the expected proton distribution in each arm (Fig. 23 left).

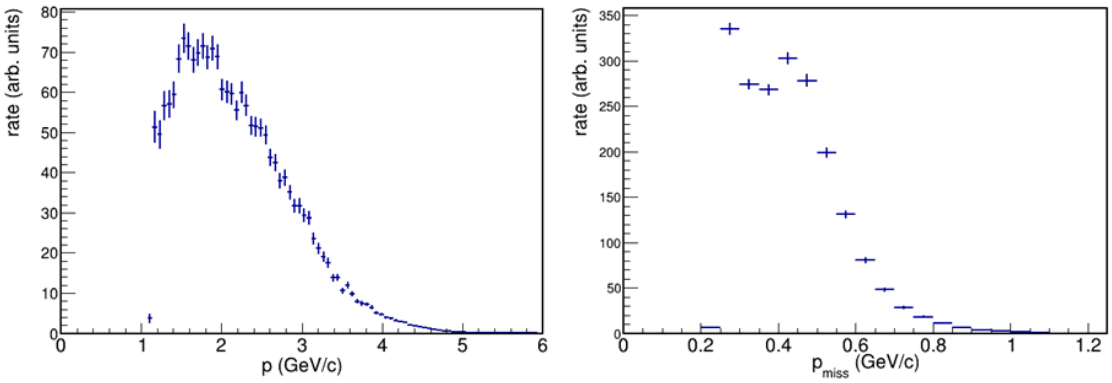

Figure 23: The simulated distribution of proton momentum in each arm (left) and the missing momentum pmiss distribution (right) as to be measured in d(p,2p).

For a beam intensity of 10^6 deuterons/sec the number of expected events that passed the cuts above and two weeks of running is summarized in Table 1. Assuming 25% σ_+, 25% σ_-, and 50% σ_0 polarization, the statistical uncertainties for A_{ZZ} for the p_{miss} bins is also shown below in Table 24.

p_{miss} bin (GeV/c)	Number of events	A_{zz} stat. uncertainty
0.25 – 0.30	81,030	0.007
0.30 – 0.35	66,220	0.007
0.35 – 0.40	64,820	0.007
0.40 – 0.45	73,200	0.007
0.45 – 0.50	67,310	0.007
0.50 – 0.55	48,050	0.009
0.55 – 0.60	31,690	0.010
0.60 – 0.65	19,390	0.013
0.65 – 0.70	11,530	0.017
0.70 – 0.75	6,800	0.023
0.75 – 0.80	4,350	0.028
0.80 – 0.85	2,620	0.037
0.85 – 0.90	1,510	0.048
0.90 – 0.95	880	0.063
0.95 – 1.00	460	0.087
Total	479,860	

Figure 24: Rate estimates for d(p,2p) for 10^6 deuterons/sec, 50% duty cycle, and 2 weeks running.

Figure 25 shows calculations by Misak Sargsian and Mark Strikman [80], and Yuri Uzikov together with fictitious data and stat. uncertainties (at high momentum) expected in two weeks of beam on target. The figure demonstrates the sensitivity of the A_{ZZ} calculation to the relativistic formalism (Light cone LC [84] vs. virtual nucleon VNA [83]) and different deuteron wave functions (CD Bonn

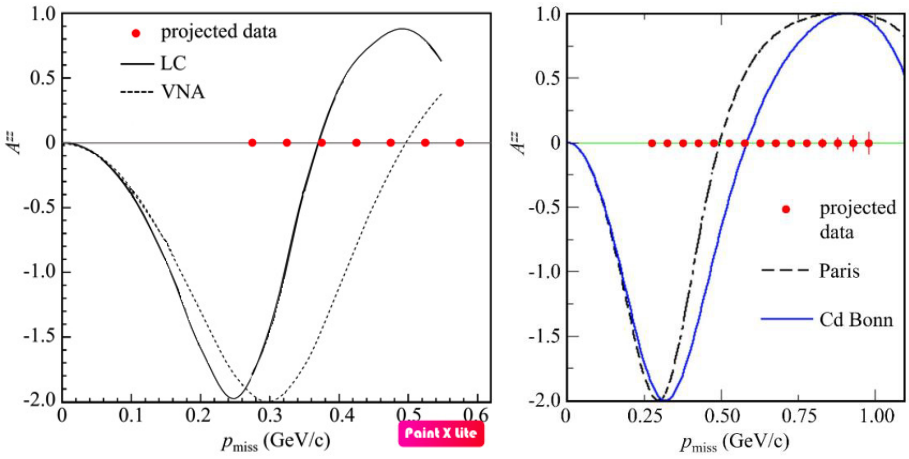

Figure 25: A_{ZZ} as a function of p_{miss} for two relativistic formalisms, light cone (LC) and virtual nucleon (VNA) (left) and for two different nuclear potentials (right). The projected data is shown by the red dots, the expected statistical uncertainties are often smaller than the points shown.

and Paris potentials). The expected statistical uncertainties show that with a reasonable beam time there are no statistical limitations to distinguishing between different models.

The large acceptance in terms of the (p,2p) missing momentum and the recoil neutron longitudinal and transverse components (α, p_T) will allow us to select and compare events which suppress FSI and others with relatively large FSI to study this important effect. The detailed selections will be finalized using our simulation and the calculations mentioned above [79, 80] after the latter will be available.

4 Phase 2: Exclusive SRC measurements

We propose to continue at JINR our international program aimed at investigating SRC effects [85, 86] with the primary objective of understanding cold, dense nuclear matter [52, 87]. The unique, high-energy ion beams, in conjunction with the dedicated SRC/HyperNIS setup, provide us with means to further explore hard quasi-elastic nucleon knockout from the beam ions in an inverse kinematics setting in coincidence with the residual fragment/fragments.

4.1 Physics goals

Cutting-edge in the SRC research field is the exploration of three-nucleon SRCs [88, 89, 90]. These investigations are of paramount importance for gaining precise insights into nuclear structure and nucleon-nucleon interactions. One key advantage of JINR in the pursuit of 3N-SRCs lies in the significantly larger cross-section of proton-proton (pp) scattering when compared to electron-proton (ep) scattering. This expanded cross-section provides a favorable environment for the search for three-nucleon SRCs. The inverse kinematics that allows to identify the A-3 residual system is also an advantage to be utilized in the search for 3N SRC signals.

To carry out studies on 3N-SRCs successfully, specific technical requirements must be met. These requirements include a high-intensity carbon-12 beam, with a rate of 107 particles per second and a momentum of approximately 3.5 GeV/c per nucleon.

4.2 Concept for HyperNIS area setup

The conceptual setup for studying SRC at HyperNIS is depicted in Fig. 26. This configuration encompasses both pre-existing components and novel additions:

- The inclusion of a second analyzing magnet significantly enhances the overall resolution for isolated ion fragments.
- A two-arm spectrometer is integrated, comprising two stations of coordinate detectors (GEM and CSC) and a substantial TOF-calorimeter on each arm. This system is purpose-built for track reconstruction of the ejected protons and precise measurement of their momenta.
- Coordinate detectors located between the two magnets and downstream serve the critical function of detecting, identifying, and measuring the momentum of the final-state and recoil ions.

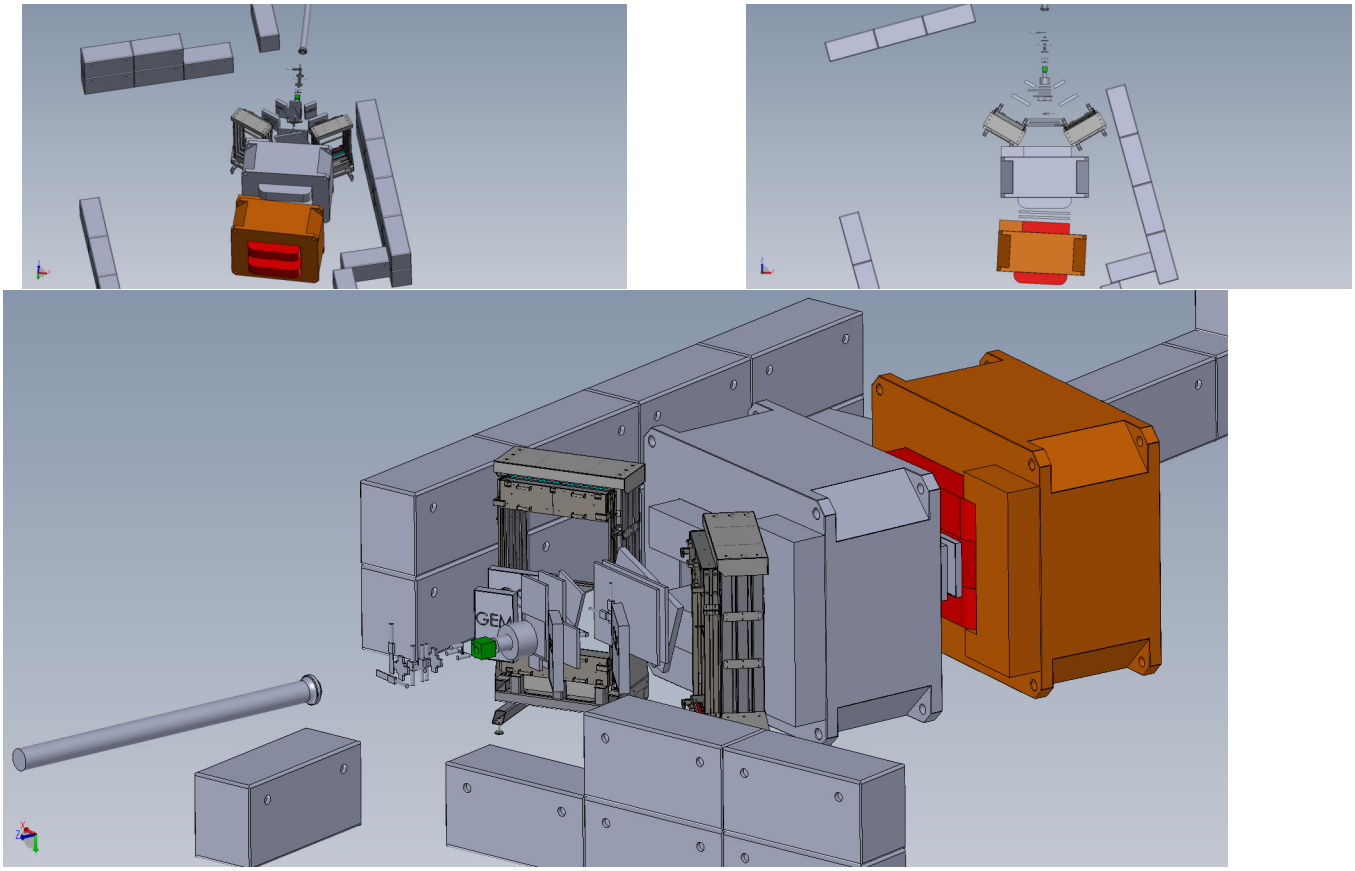

Figure 26: A CAD model showing different views of the conceptual design of the combined spectrometer for two experiments: HyperNIS and SRC. The major modifications for the SRC experiment are the second dipole magnet (shown in orange) and the two-arm spectrometer located upstream the magnets. These SRC additions are compatible with the HyperNIS setup.

These modifications to the original HyperNIS setup can be seamlessly incorporated without significant disruption to existing equipment, thereby facilitating the concurrent operation of multiple experiments in the same area. However, the installation of the second dipole magnet necessitates engineering assessments and preparatory work, including floor reinforcement in the HyperNIS area. These tasks are time-consuming, and initiating this work ahead of the final proposal, which will be based on the 2022 results pending approval, is contemplated.

Regarding detector availability, TOF-calorimeter detectors with Front-End Electronics (FEE) are repurposed from the SRC/BM@N setup, while the coordinate detectors for the arms may be sourced

locally at LHEP. However, the coordinate detectors situated between and downstream of the magnets will require manufacturing. Notably, the Data Acquisition (DAQ) system is not yet in place.

The maximum attainable beam momentum for ion beams at the HyperNIS area is 9 GeV/c/charge, equivalent to 4.5 GeV/c/nucleon for carbon beams. The SRC measurement calls for a beam momentum within the 3-3.5 GeV/c/nucleon range. Furthermore, accommodating ion beams with an intensity of up to 10^7 ions/s necessitates upgrades to radiation protection measures in the HyperNIS area. It is important to note that we intend to continue utilizing the cryogenic liquid hydrogen target previously employed in the SRC measurements at BMN in 2022 at HyperNIS.

4.3 Preliminary simulation studies

We conducted a preliminary simulation study for the HyperNIS setup. Assuming a carbon-12 beam we estimated the momentum resolution for fragments emitted along the beam and the geometrical acceptance of the two magnets.

In the BmnRoot software, the BM@N analyzing magnet (SP-41) was adapted to match the SP-40 magnet used at the HyperNIS area. The SP-40 magnet's pole length is 1.5 meters. We scaled the magnetic field map to align with the working magnetic field of 0.6 T (at the highest possible working current of 1100 A). We introduced a second identical magnet in the simulation, with a center-to-center distance of 375 cm. This second magnet was rotated by 4 degrees relative to the first magnet and the global z-axis to enhance the transport of charged fragments (see Fig. 27).

The particles are generated at 550 cm from the center of the first magnet. The trajectories of the fragments, as measured by the silicon detectors upstream of the magnets and the generic detector stack downstream of the magnets, are utilized to derive the P/Z (momentum per charge) ratio using a Multidimensional Fit reconstruction. The two straight portions of the particle trajectory are used as input for a simulation-based approach. We assumed spatial uncertainties of 50 micrometers for the silicon detectors and 200 micrometers for the generic detector stack.

To estimate the momentum resolution for carbon-12 and helium-6 ions (as an extreme P/Z ratio), we used a beam with a circular spot (radius of 4 cm) and a direction defined by Gaussian distributions of px and py with a standard deviation of 150 MeV/c (equivalent to 5 mrad). The absolute momentum spread was defined as (P / 1.1, P * 1.1), where P is the nominal momentum value. The resulting momentum resolutions are presented in Table 2. For comparison, the experimentally achieved momentum resolution in the 2018 SRC experiment at JINR, conducted at the BM@N setup, was 1.6%.

Table 2: Table of the momentum resolution for different ion species.

ion	momentum P, GeV/c per nucleon	standard deviation σ	σ/P [%]
^{12}C	3.5	0.25	0.6
^{12}C	2.5	0.16	0.55
^{6}He	3.5	0.13	0.9
^{6}He	2.5	0.18	0.8

The primary factor affecting the geometrical acceptance of secondary particles traveling along the beam is the vertical acceptance of the SP-40 magnets. Each SP-40 magnet has dimensions of 3 m

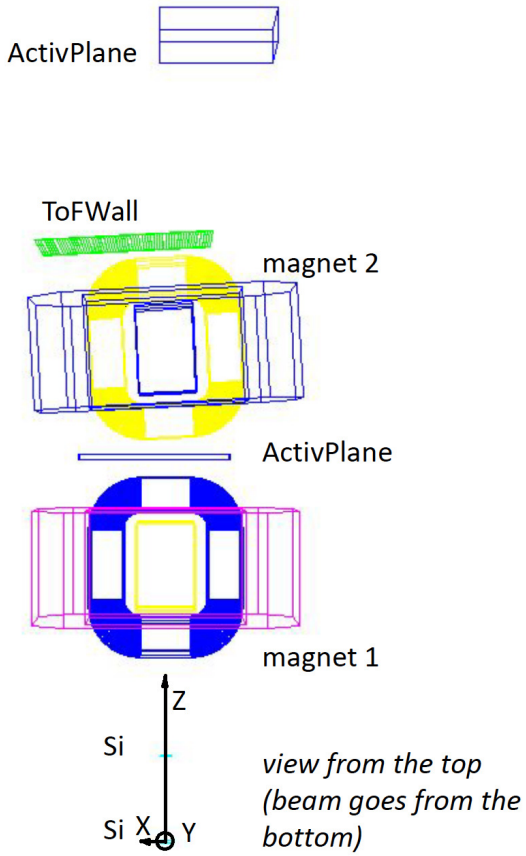

Figure 27: A top-down view of the simplified experimental setup, with the beam entering from bottom to top. The two SP-40 magnets are labeled as magnet 1 and magnet 2. The active detector system comprises two silicon detectors upstream of the magnets and a generic detector stack downstream of the magnets.

along the beam. Considering a 1-meter passageway between the magnets, the total length of the two magnets along the beam is 7 m. The two-arm spectrometer should be positioned upstream of the first magnet, with an arm length of approximately 5 m. This results in a total distance from the target to the exit of the second magnet of about 12 m.

The current vertical opening of the second SP-40 magnet is 40 cm but it can be increased. The geometrical acceptance, based on the magnet opening, is quite limited, as listed in Table 3. The horizontal acceptance is determined by the horizontal dimension of the magnet opening, which is 2.6 m. The acceptance in the horizontal direction for target particles is then 6.5 degrees.

Table 3: Table of the geometrical acceptance in vertical direction for the particles originating in the target for different vertical openings of the second SP-40 magnet.

Table 4: Geometrical acceptance in the vertical direction for particles originating in the target, for different vertical openings of the second SP-40 magnet.

total vertical acceptance [m]	geometrical acceptance [degrees]
0.4	1.01
0.5	1.26
0.68	1.73

References

[1] M. Agnello *et al.* (FINUDA Collaboration), Phys. Rev. Lett. **108**, 042501 (2012).
[2] E. Botta, Nucl. Phys. A **914**, 119 (2013).
[3] M. Agnello *et al.*, Nucl. Phys. A **881**, 269 (2012).
[4] H. Sugimura *et al.* (J-PARC E10 Collaboration), Phys. Lett. B **729**, 39 (2014).
[5] A. U. Abdurakhimov *et al.*, Nuovo Cim. A **102**, 645 (1989).
[6] S. Avramenko *et al.*, Nucl. Phys. A **547**, 95 (1992).
[7] H. Bandō *et al.*, Nucl. Phys. A **501**, 900 (1989).
[8] H. Bandō, T. Motoba, and J. Žofka , Int. J. Mod. Phys. A **5**, 4021 (1990).
[9] S. Piano, JPS Conf. Proc. **17**, 021004 (2017).
[10] C. Rappold and T. Saito, JPS Conf. Proc. **17**, 021003 (2017).
[11] H. Kamada *et al.*, Phys. Rev. C **57**, 1595 (1998).
[12] T. Motoba *et al.*, Nucl. Phys. A **534**, 597 (1991).
[13] B. Donigus, AIP Conf. Proc. **2130**, 020017 (2019).
[14] L. Adamczyk *et al.* (STAR Collaboration), Phys. Rev. C **97**, 054909 (2018).
[15] ALICE Collaboration, arXiv: 2209.07360 [nucl-ex].
[16] M. S. Abdallah *et al.* (STAR Collaboration), arXiv: 2110.09513 [nucl-ex].
[17] Yu. A. Batusov *et al.*, Phys. Part. Nucl. **36**, 169 (2005) [Fiz. Elem. Chast. Atom. Yadra **36**, 319 (2005)].
[18] T. R. Saito *et al.*, *Proc. of the IX International Conference on Hypernuclear and Strange Particle Physics (HYP06), 2006, Mainz*, ed. by J. Pochodzalla and Th. Walcher, Springer, Berlin, Heidelberg (2007), 171.
[19] C. Rappold *et al.*, Nucl.Phys. A **913**, 170 (2013).
[20] S. A. Avramenko *et al.*, Nucl. Phys. A **585**, 91 (1995).
[21] Z. Arzoumanian *et al.*, Astrophys. J. Suppl. **235**, 37 (2018); J. Antoniadis *et al.*, Science **340**, 1233232 (2013); H. T. Cromartie *et al.*, Nature Astronomy **4**, 72 (2019).
[22] D. Logoteta, I. Vidana, and I. Bombaci, Eur. Phys. J. A **55**, 207 (2019) [arXiv: 1906.11722].
[23] A. Sakaguchi, JPS Conf. Proc. **17**, 011007 (2017).
[24] E. Hiyama *et al.*, Nucl. Phys. A **908**, 29 (2013).
[25] A. Gal and D.J. Millener, Phys. Lett. B **725**, 445 (2013) [arXiv: 1305.6716].
[26] B. F. Gibson and I. R. Afnan, Nucl. Phys. A **914**, 179 (2013); Few-Body Systems **55**, 913 (2014).
[27] L. Majling, Nucl. Phys. A **585**, 211 (1995).

[28] L. Majling, *Proc. of the IX International Conference on Hypernuclear and Strange Particle Physics (HYP06), 2006, Mainz*, ed. by J. Pochodzalla and Th. Walcher, Springer, Berlin, Heidelberg (2007), 149.
[29] R. H. Dalitz and R. Levi Setti, Nuovo Cimento **30**, 489 (1963).
[30] Y. Akaishi and T. Yamazaki, Frascati Phys. Ser. **16**, 59 (1999).
[31] K. S. Myint and Y. Akaishi, Progr. Theor. Phys. Suppl. **146**, 599 (2003).
[32] S. Shinmura *et al.*, J. Phys. G **28**, L1 (2002).
[33] S. A. Avramenko *et al.*, JINR Communication P1-91-206, Dubna (1991).
[34] J. Lukstins, Nucl. Phys. A **691**, 491 (2001).
[35] S. V. Afanasiev *et al.*, *Proc. of the IX International Conference on Hypernuclear and Strange Particle Physics (HYP06), 2006, Mainz*, ed. by J. Pochodzalla and Th. Walcher, Springer, Berlin, Heidelberg (2007), 165.
[36] M. V. Evlanov *et al.*, Nucl. Phys. A **632**, 624 (1998); Part. Nucl. Lett. **105**, 5 (2001).
[37] L. Majling and Yu. Batusov, Nucl. Phys. A **691**, 185c (2001).
[38] M. M. Block and R. H. Dalitz, Phys. Rev. Lett. **11**, 96 (1963).
[39] R. A. Salmin, O. V. Borodina, A. I. Maksimchuk, and V. L.Rapatsky, The talk at the LHE JINR Seminar on relativistic nuclear physics, June 06, 2007.
[40] V. D. Aksinenko *et al.*, *Proc. of XIX International Baldin Seminar on High Energy Physics Problems "Relativistic Nuclear Physics and Quantum Chromodynamics", Dubna, September 29 - October 4, 2008)*, JINR, Dubna, 2008, 155.
[41] A. V. Averyanov *et al.*, Phys. Part. Nuclei Lett. **16**, 826 (2019).
[42] M. Patsyuk *et al.* (BM@N Collaboration), Nature Physics **17**, 693 (2021) [arXiv: 2102.02626].
[43] L. L. Frankfurt and M. I. Strikman, Phys. Rep. **76**, 215 (1981).
[44] L. Frankfurt and M. Strikman, Phys.Rept. **160**, 235 (1988).
[45] C. Cioffi degli Atti, Phys. Rep. 590, 1-85 (2015).
[46] O. Hen et al, Rev. Mod. Phys. 89, 045002 (2017).
[47] O. Hen *et al.*, Science 346, 614 (2014), arXiv: 1407.8175 [nucl-ex].
[48] M. Duer et al. (CLAS), Nature 560, 617 (2018).
[49] A. Schmidt *et al.* (CLAS Collaboration), Nature **578**, 540 (2020).
[50] B. Schmookler et al. (CLAS), Nature 566, 354-358 (2019).
[51] I. Korover et al. (JLab Hall A), Phys. Rev. Lett. 113, 022501 (2014).
[52] R. Subedi et al., Science 320, 1476 (2008).
[53] O. Hen et al. (CLAS), Phys. Lett. B 722, 63 (2013).
[54] R. Schneor et al. (JLab Hall A), Phys. Rev. Lett. 99, 072501 (2007).
[55] E. Piasetzky et al., Phys. Rev. Lett. 97, 162504 (2006).
[56] A. Tang et al., Phys. Rev. Lett 90, 042301 (2003).
[57] M. Duer et al. (CLAS), Phys. Rev. Lett. 122, 172502 (2019).
[58] R. Schiavilla et al., Phys. Rev. Lett. 98, 132501 (2007).
[59] M. Sargsian et al., Phys. Rev. C 71m 044615 (2005).
[60] M. Alvioli, C. Cioffi degli Atti, H. Morita, Phys. Rev. Lett. 100, 162503 (2008).
[61] M. Alvioli, C. Cioffi degli Atti, H. Morita, Phys. Rev. C 94, 044309 (2016).
[62] M. Alvioli et al., Phys. Rev. C 85, 201001 (2012).
[63] R. Weiss, B. Bazak, N. Barnea, Phys. Rev. C 92, 054311 (2015).
[64] R. Weiss, R. Cruz-Torres et al., Phys. Lett. B 780, 211-215 (2018).
[65] R. Cruz-Torres et al., Nature Physics 17, 306-310 (2021).
[66] A. Schmidt et al. (CLAS), Nature 578, 540-544 (2020).
[67] J. Pybus et al., Phys. Lett. B 805, 135429 (2020).
[68] E. O. Cohen et al. (CLAS), Phys. Rev. Lett. 121, 092501 (2018).
[69] K. Sh. Egiyan et al. (CLAS), Phys. Rev. C 68, 014313 (2003).

[70] N. Fomin et al., Phys. Rev. Lett. 108, 092502 (2012).
[71] L. L. Frankfurt and M. I. Strikman, Nucl. Phys. B **148**, 107 (1979).
[72] W. W. Buck and F. Gross, Phys. Rev. D **20**, 2361 (1979).
[73] R. Machleidt, Phys. Rev. C 63, 024001 (2001).
[74] R. B. Wiringa, V. G. J. Stoks, R. Schiavilla, Phys. Rev. C 51, 38 (1995).
[75] L. Frankfurt, M. Strikman, Nucl. Phys. A 405, 557-580 (1983).
[76] I. Paschier et al., Phys. Rev. Lett. 88, 102302 (2002).
[77] E. Long, J. Phys.: Conf. Ser. 543, 012010 (2014).
[78] L. L. Frankfurt *et al.*, Z. Phys. A **352**, 97 (1995); Phys. Lett. B 369, 201 (1996).
[79] A. B. Larionov, Phys. Rev. C **107**, 014605 (2023).
[80] M. Sargsian, M. Strikman, J. Phys. Conf. Ser. 543, 012009 (2014).
[81] Alexey Larionov, private communication.
[82] M. Sargsian, F. Vera, Phys. Rev. Lett. 130, 112502 (2023).
[83] L. Frankfurt et al., Phys. Rev. C 48, 2451 (1993).
[84] M. M. Sargsian, Phys. Rev. C 82, 014612 (2010).
[85] O. Hen et al., Rev. Mod. Phys. 89, 045002 (2017).
[86] J. Arrington et al., Rev. of Nucl. and Part. Sc. 72, 307-337 (2022).
[87] L. Frankfurt et al., Int. J. of Mod. Phys. A 23, 20 (2008).
[88] M. M. Sargsian et al., Phys. Rev. C 100, 044320 (2019).
[89] R. Weiss et al., Phys. Rev. C 108, L021301 (2023).
[90] D. B. Day et al., Phys. REv. C 107, 014319 (2023).

2.3 Estimated completion date 2024-2028

2.4 Participating JINR laboratories VBLHEP

2.4.1 MICC resource requirements

Computing resources	**Distribution by year**				
	1st year	2nd year	3rd year	4th year	5th year
Data storage (TB) -EOS -Tapes	0	0	0	0	0
Tier 1 (CPU core hours)	0	0	0	0	0
Tier 2 (CPU core hours)	0	0	0	0	0
SC Govorun (CPU core hours) - CPU - GPU	0	0	0	0	0
Clouds (CPU cores)	0	0	0	0	0

2.5 Participating countries, scientific and educational organizations

Organization	Country	City	Participants	Type of agreement
TAU	Israel	Tel Aviv	Kalbow J.	
TAU	Israel	Tel Aviv	Johansson G.	
MIT	USA	Kembrige	Hen O.	
RCNP	Japan	Osaka	Nakano T.	
CTU	Czech Republic	Prague	Pospishil S.	

2.6 Key partners (those collaborators whose financial, infrastructural participation is substantial for the implementation of the research program. An example is JINR's participation in the LHC experiments at CERN).

3. Manpower

3.1. Manpower needs in the first year of implementation

№№ n/a	Category of personnel	JINR staff, amount of FTE	JINR Associated Personnel, amount of FTE
1.	research scientists	9.81	
2.	engineers	5	
3.	specialists		
4.	office workers		
5.	technicians		
	Total:	**14.81**	

3.2. Available manpower

3.2.1. JINR staff

No.	Category of personnel	Full name	Division	Position	Amount of FTE
1.	research scientists	Aksinenko V.D.	VBLHEP		1
		Atovullaev T.	VBLHEP		1
		Averyanov A.V.	VBLHEP		0.89
		Fechtchenko A.A.	VBLHEP		0.69
		Gertsenberger S.V.	VBLHEP		0.1
		Khvorostukhin A.S.	VBLHEP		1
		Korotkova A.M.	VBLHEP		0.94
		Krivenkov D.O.	VBLHEP		0.7
		Lukstins J.	VBLHEP		0.45
		Nepochatykh S.M.	VBLHEP		1
		Patsyuk M.A.	VBLHEP		1
		Strokovsky E.A.	VBLHEP		0.84
		Tereschenko V.V.	DLNP		0.2
2.	engineers	Atovullaeva A.	VBLHEP		1
		Bochkova A.G.	VBLHEP		0.5
		Okhrimenko O.V.	VBLHEP		1
		Parfenova N.G.	VBLHEP		0.5
		Plyashkevich S.N.	VBLHEP		1
		Salamatin A.V.	VBLHEP		1
3.	specialists				
4.	technicians				
	Total:				**14.81**

3.2.2. JINR associated personnel

No.	Category of personnel	Partner organization	Amount of FTE
1.	research scientists		
2.	engineers		
3.	specialists		
4.	technicians		
	Total:		

4. Financing

4.1 Total estimated cost of the project/LRIP subproject The total cost estimate of the project (for the whole period, excluding salary). The details are given in a separate table below.

4.2 Extra funding sources Expected funding from partners/customers – a total estimate.

Project (LRIP subproject) Leader _____ / _____ /

Date of submission of the project (LRIP subproject) to the Chief Scientific Secretary: _____
Date of decision of the laboratory's STC: 21.11.23 document number: _____
Year of the project (LRIP subproject) start: _____
(for extended projects) — Project start year: _____

Proposed schedule and resource request for the Project / LRIP subproject

Expenditures, resources, funding sources			Cost (thousands of US dollars)/ Resource requirements	Cost/Resources, distribution by years				
				1st year	2nd year	3rd year	4th year	5th year
		International cooperation	75	15	15	15	15	15
		Materials	125	25	25	25	25	25
		Equipment, Third-party company services						
		Commissioning						
		R&D contracts with other research organizations						
		Software purchasing	10	2	2	2	2	2
		Design/construction						
		Service costs (*planned in case of direct project affiliation*)						
Resources required	Standard hours	Resources						
		– the amount of FTE,		15	15	15	15	15
		– accelerator/installation,		360	360	360	360	360
		– reactor,...						
Sources of funding	JINR Budget	JINR budget (*budget items*)						
	Extra funding (supplementary estimates)	Contributions by partners Funds under contracts with customers Other sources of funding						

Project (LRIP subproject) Leader _____ / _____ /

Laboratory Economist _____ Морозов В.В.

APPROVAL SHEET FOR PROJECT / LRIP SUBPROJECT

HyperNIS-SRC

(HyperNuclear Intrinsic Strangeness and Short Range Correlations)

Theme code 02-1-1086-2009

D.O. Krivenkov, J. Lukstins

AGREED

	SIGNATURE	NAME	DATE
JINR VICE-DIRECTOR			
CHIEF SCIENTIFIC SECRETARY			
CHIEF ENGINEER			
LABORATORY DIRECTOR		Butenko A.V.	
CHIEF LABORATORY ENGINEER		Somin N.V.	
LABORATORY SCIENTIFIC SECRETARY THEME / LRIP LEADER		Strokovsky E.A.	
PROJECT / LRIP SUBPROJECT LEADER		Krivenkov P.O.	
PROJECT / LRIP SUBPROJECT LEADER		Lukstiņš	

APPROVED BY THE PAC

SIGNATURE	NAME	DATE